

1 **Response to comments**

2 The authors thank the reviewers for their constructive comments, which provide the basis to improve the quality of
3 the manuscript and dataset. We address all points in detail and reply to all comments here below. We also updated
4 SCDNA from V1 to V1.1 on Zenodo based on the reviewer's comments. The modifications include adding station
5 source flag, adding original files for location merged stations, and adding a quality control procedure based on the
6 final SCDNA. SCDNA estimates are generally consistent between the two versions, with the total number of stations
7 reduced from 27280 to 27276.

8

9 **Reviewer 1**

10 **General comment**

11 The manuscript presents and advertises a very interesting dataset of temperature and precipitation observation
12 collected over several years in North America. The work is certainly well suited for the readership of ESSD and it is
13 overall very important for the meteorological and climatological community. Furthermore, creation of quality
14 controlled databases is an important contribution to the scientific community in the age of data science. I have a few
15 points to consider before publication, which I recommend, listed below.

16 1. Measurement instruments: from my background, I am much closer to the instruments themselves (and their
17 peculiarities and issues), as hardware tools. What I missed here was a description of the stations and their instruments.
18 Questions like: which are the instruments deployed in the stations? How is precipitation measured (tipping buckets?
19 buckets? Weighing gauges? Note for example that some instruments may have biases when measuring snowfall while
20 others may not)? How is it temperature measured? How is this different from station to station in your database?

21 Response: We have added the descriptions of measurement instruments in both the manuscript and dataset
22 documentation. Since a complete introduction to the specifications and the evolution of measurement instruments in
23 North America is not trivial, we only provide a general introduction here, and guide readers to the official sources for
24 more comprehensive knowledge (such as design purpose, instrument structure, accuracy for rain/snow, inter-
25 instrument comparison) in the manuscript and dataset page. As station hardware varies among countries, we
26 successively introduce the overall situations in Canada, U.S., and Mexico as below.

27 For Canada, the Type-B rain gauge is used since 1970s for most stations by Environment Canada (Devine and Mekis,
28 2008; Wang et al., 2017). Tipping bucket and weighing gauges are also used in some stations (Metcalfé et al., 1997).
29 For snowfall measurement, Nipher-shielded snow gauges were introduced at nearly 300 synoptic stations in the early
30 1960s, while most snow observation stations still rely on ruler measurements ([https://www.canada.ca/en/environment-
31 climate-change/services/sky-watchers/weather-instruments-tour.html](https://www.canada.ca/en/environment-climate-change/services/sky-watchers/weather-instruments-tour.html)). For temperature, weather observers use as
32 many as 4 different thermometers mounted inside the Stevenson screen. Maximum and minimum thermometers use
33 mercury and alcohol, respectively ([https://www.canada.ca/en/environment-climate-change/services/sky-
34 watchers/weather-instruments-tour/thermometers-thermistors.html](https://www.canada.ca/en/environment-climate-change/services/sky-watchers/weather-instruments-tour/thermometers-thermistors.html)). However, detailed metadata for an individual
35 station is hard to obtain (e.g., see the detailed analysis of Whitfield (2014) for the station 3053600 in Kananaskis,
36 Alberta).

37 For the U.S.A., station data are provided by many agencies/programs. The sources are denoted in SCDNA using the
38 source flags provided in the GHCN-D dataset. For stations from the Cooperative Observer Program (COOP), the
39 instruments are summarized in <https://www.weather.gov/ilx/coop-equipment>. The Standard Rain Gage (SRG) is used,

40 and the method for measuring rainfall and snowfall is summarized in https://www.weather.gov/iwx/coop_8inch. For
41 stations from Community Collaborative Rain, Hail, and Snow (CoCoRaHS), a 4-inch diameter rain gauge is used
42 (<https://www.cocorahs.org/Content.aspx?page=rain>). For the U.S. Automated Surface Observing System (ASOS),
43 heating Heated Tipping Bucket (HTB) and hygrothermometer are used for most stations, and there is a transition from
44 HTB to All Weather Precipitation Accumulation Gauge (AWPAG) since 2004
45 (<https://www.weather.gov/asos/ASOSImplementation>, file:///Users/localuser/Downloads/ASOS_guide_1998.pdf).
46 For NCEI Reference Network Database, a combination of weighing gauge, precipitation detector, and tipping bucket
47 gauge are used, and air temperature is measured using three platinum resistance thermometers housed in fan aspirated
48 solar radiation shields (<https://www.ncdc.noaa.gov/crn/instruments.html>). For SNOTEL, storage-type gage or tipping
49 bucket is used, and temperature is measured using shielded thermistor
50 (https://www.wcc.nrcs.usda.gov/snotel/snotel_sensors.html,
51 https://www.wcc.nrcs.usda.gov/about/mon_automate.html). For Remote Automatic Weather Station (RAWS), THS-
52 3 temperature and humidity sensor and RG-T tipping bucket rain gauge are used
53 (https://www.fs.fed.us/eacc/library/docs/RAWS_WIMS_Guide.pdf, [https://ftsinc.com/fixed-remote-automated-
54 weather-station](https://ftsinc.com/fixed-remote-automated-weather-station)). For High Plains Regional Climate Center real-time data, tipping bucket or rain gauge is used
55 (<https://hprcc.unl.edu/awdn/index.php>).

56 For Mexico, the automatic weather station, which is a set of electrical and mechanical devices that perform
57 measurements of meteorological variables automatically (WMO Reference 182) are used by Servicio Meteorológico
58 Nacional. (<https://smn.conagua.gob.mx/es/observando-el-tiempo/estaciones-meteorologicas-automaticas-ema-s>).

59 A useful database, the Historical Observing Metadata Repository (HOMR), is maintained by NOAA NCEI
60 (<https://www.ncdc.noaa.gov/data-access/land-based-station-data/station-metadata>). Users can find detailed
61 information of a station using station ID provided by different station sources, including SCDNA. For example, COOP
62 station USC00244302 measures precipitation using SRG from 2000 to 2018-10-4 and SRG-STN since 2018-10-4.
63 However, instrument information could be missing for many stations outside U.S.

64 We added a paragraph in Section 2.1: “Many types of precipitation and temperature measurement instruments are
65 used at stations from different sources. For example, the Type-B rain gauge is used by Environment Canada since
66 1970s for most weather stations (Devine and Mekis, 2008; Wang et al., 2017), while tipping bucket and weighing rain
67 gauges are also used in some stations (Metcalf et al., 1997). Nipher-shielded snow gauges have been used by some
68 synoptic stations, while ruler measurements are still used by more stations (Mekis and Brown, 2010). Station data in
69 U.S. are from many organizations or programs with different instrument configurations. For instance, the standard
70 rain gauge is used by the Cooperative Observer Program while Snow Telemetry uses storage-type gauges or tipping
71 buckets. A better understanding of instrument specifications and historical changes is important for climate studies
72 (Pielke Sr et al., 2007; Whitfield, 2014; Ma et al., 2019). A detailed summary of station instruments is provided in the
73 documentation of the dataset (<https://doi.org/10.5281/zenodo.3953310>).”

74

75 Reference:

76 Devine, K. A., & Mekis, E. (2008). Field accuracy of Canadian rain measurements. *Atmosphere-ocean*, 46(2), 213-
77 227.

78 Mekis, É., & Brown, R. (2010). Derivation of an adjustment factor map for the estimation of the water equivalent of
79 snowfall from ruler measurements in Canada. *Atmosphere-ocean*, 48(4), 284-293.

80 Metcalfe, J. R., B. Routledge, and K. Devine. 1997. Rainfall measurement in Canada: Changing observational methods
81 and archive adjustment procedures. *Journal of Climate* 10: 92-101.

82 Pielke Sr, R., Nielsen-Gammon, J., Davey, C., Angel, J., Bliss, O., Doesken, N., ... & Hale, R. (2007). Documentation
83 of uncertainties and biases associated with surface temperature measurement sites for climate change assessment.
84 *Bulletin of the American Meteorological Society*, 88(6), 913-928.

85 Whitfield, P. H. 2014. Climate station analysis and fitness for purpose assessment of 3053600 Kananaskis, Alberta.
86 *Atmosphere-Ocean* 52(5): 363-383.

87 Wang, X. L., Xu, H., Qian, B., Feng, Y., & Mekis, E. (2017). Adjusted daily rainfall and snowfall data for Canada.
88 *Atmosphere-Ocean*, 55(3), 155-168.

89 2. Codes: have you considered adding a little reader with a few capabilities, as additional tool for the interested users?

90 Response: We have added more detailed descriptions on GitHub
91 (<https://github.com/tgq14/GapFill/blob/master/README.md>). The functions and their usage of different modules are
92 introduced in Readme.md. Users can utilize the entire or part of the code package with the help of comments contained
93 in scripts.

94 Minor/Details

95 1. P2: as trivial as it can be, it is worth to define the term "station".

96 Response: We added the definition. The revised sentence in P2 is "Many methods have been developed to estimate
97 missing observations and reconstruct time series of meteorological stations that provide point-scale regular
98 observations of atmospheric conditions".

99 2. P3, L96: Why exactly the variables of Tmin, Tmax, and precipitation have been chosen? Is it a matter of (lack of)
100 availability of other measurements? (humidity, wind, etc). I just suggest to clarify.

101 Response: We selected the three variables for two reasons. First, as you have indicated, precipitation, Tmin and Tmax
102 are the most common variables provided by meteorological stations, while other variables such as wind or humidity
103 are less common. Second, most previous studies focus on precipitation and temperature, while other variables attract
104 less attention. Thus, whether our methodology will work for other variables needs further investigation. We added
105 explanation in the first paragraph in P3: "The three variables are selected because (1) most stations measure
106 precipitation and temperature, while other variables, such as humidity and wind speed are measured at fewer stations,
107 and (2) precipitation and temperature data are fundamental inputs for hydrological modeling."

108 We also added discussion on involving other variables in future work in Section 5.4.

109 3. Is precipitation the daily amount? I probably missed this information.

110 Response: Yes, it is. We added explanation in the first paragraph in Section 2.1: "In this dataset, precipitation is the
111 daily amount."

112

113 **Reviewer 2**

114 This study develops a very useful dataset (SCDNA) of serially complete precipitation and temperature in North
115 America. The dataset will benefit researchers in various fields with the long-term and gap-filled station data collected
116 from multiple sources. The sophisticated framework for imputing missing values is well designed, which can be
117 potentially applied in other regions of the world for the production of regional or even global serially complete datasets.
118 From my perspective, the paper can be published on ESSD after the minor revisions, and I also have a few comments
119 as below.

120 1. The differences between SCDNA and MSWEP show distinct differences along the boundaries of CONUS and
121 Canada. Can you provide more detailed explanation about how observation time inconsistency causes this problem?

122 Response: MSWEP merges data from satellite products, reanalysis models and ground observations. Station data in
123 different regions could have different observation time. To match station and reanalysis/satellite data, MSWEP
124 calculates daily grid- and gauge-based time series, with the grid-based time series shifted by offsets of -36, -33,
125 -30, ..., +30, +33, and +36 h. Then, the temporal offset with the highest correlation is used to calculate 24-h
126 accumulation of daily precipitation (Beck et al., 2019). Therefore, the final MSWEP estimates do not necessarily
127 correspond to the raw observation of stations. For CONUS and Canada, the temporal offset is different and thus the
128 mismatch between MSWEP and original station data is different.

129 We added an explanation in the third paragraph in Section 4.4: "Fig. 15 shows notable differences between MSWEP
130 and SCDNA at the Canada-USA border and the USA-Mexico border. This is because MSWEP infers gauge reporting
131 time by searching for the highest correlation between gauge data and the temporally shifted reanalysis/satellite
132 estimates (Beck et al., 2019). The estimated temporal shift could vary with countries, which results in distinct
133 differences of station-based evaluation results along national boundaries."

134 Reference:

135 Beck, H. E., Wood, E. F., Pan, M., Fisher, C. K., Miralles, D. G., Van Dijk, A. I., ... & Adler, R. F. (2019). MSWEP
136 V2 global 3-hourly 0.1 precipitation: methodology and quantitative assessment. *Bulletin of the American
137 Meteorological Society*, 100(3), 473-500.

138 2. The paper said "Outputs from three reanalysis products (ERA5, JRA-55, and MERRA-2) provided auxiliary
139 information to estimate station records and were also used as an assessment benchmark. ". Can you give more
140 explanation why you selected reanalysis products for benchmark?

141 Response: We choose the three products because (1) they are produced by representative reanalysis models from
142 organizations in U.S., Europe, and Japan, and (2) they or their predecessors (ERA-Interim, JRA-25, and MERRA)
143 have are been widely used by previous studies (e.g., Sun et al., 2018). The three reanalysis products are used as
144 benchmark because they are widely used as the source of long-term precipitation and temperature data and have been
145 applied to support infilling and reconstruction in this study.

146 We added an explanation in Section 2.2: "The three products are chosen because they are representative products from
147 different international organizations and they or their predecessor (ERA-Interim, JRA-25, and MERRA) have are been
148 widely used by researchers."

149 Reference:

150 Sun, Q., Miao, C., Duan, Q., Ashouri, H., Sorooshian, S., & Hsu, K. L. (2018). A review of global precipitation data
151 sets: Data sources, estimation, and intercomparisons. *Reviews of Geophysics*, 56(1), 79-107.

152 3. The period from 1979 to 2018 is total 40 years. Numbers of stations with only at least 8-year records are shown in
153 Table 1. Why only 8-year period records are showed? Are only stations with at least 8-year precipitation or Tmin and
154 Tmax records between 1979 to 2018 utilized to evaluate the performance? Is there some difference between 8-year
155 records and total records for evaluation?

156 Response: For the first question, we only show 8-year records because according to our sensitivity analysis, eight
157 years are enough to ensure gap filling is generally reliable (Figure S1). Using a higher period threshold can improve
158 the quality of the final dataset but will reduce the number of stations.

159 For the second question, yes, only stations with at least eight-year records are used for evaluation to be consistent with
160 inputs.

161 For the third question, our evaluation is based on 30% samples of each station. For example, if a station has 8-year/40-
162 year observations, the validation samples are about 2.4-year/12-year. Therefore, the evaluation period length could be
163 different for different stations. According to our results (Figures 6 and 12), the spatial distributions of accuracy metrics
164 and contribution ratios are smooth, indicating that the difference between 8-year records and total records for
165 evaluation is not evident. We added explanation in Step-5 in Section 3.3.3: “Although the evaluation samples are
166 different among stations, the results are reliable and stable as shown in the results section.”

167 4. Precipitation and minimum/maximum temperature are very widely used in hydrometeorological studies. I think
168 probably this is why the three variables are chosen. Considering meteorological stations can usually measure more
169 variables which also suffer from missing values, expanding this work to other variables would be very interesting for
170 future studies. I suggest that the authors add some discussion about the applicability of your method to other variables.

171 Response: Thank you for this suggestion. Expanding this work to other variables will be an interesting study. We
172 added discussion in Section 5.4: “Furthermore, other variables such as wind and humidity observed by stations also
173 suffer from the same problems faced by precipitation and temperature. Future studies should explore whether the
174 current methodology is applicable to other variables. A SCD covering more variables would be useful for research in
175 various fields.”

176

SCDNA: a serially complete precipitation and temperature dataset for North America from 1979 to 2018

Guoqiang Tang^{1,2}, Martyn P. Clark^{1,2}, Andrew J. Newman³, Andrew W. Wood³, Simon Michael Papalexiou^{2,4}, Vincent Vionnet⁵, and Paul H. Whitfield^{1,2}

¹University of Saskatchewan Coldwater Lab, Canmore, Alberta, Canada

²Centre for Hydrology, University of Saskatchewan, Saskatoon, Saskatchewan, Canada

³National Center for Atmospheric Research, Boulder, Colorado

⁴Department of Civil, Geological and Environmental Engineering, University of Saskatchewan, Saskatchewan, Canada

⁵Environmental Numerical Research Prediction, Environment and Climate Change Canada, Dorval, Quebec, Canada

Correspondence to: Guoqiang Tang (guoqiang.tang@usask.ca)

Abstract: Station-based serially complete datasets (SCDs) of precipitation and temperature observations are important for hydrometeorological studies. Motivated by the lack of serially-complete station observations for North America, this study seeks to develop a SCD from 1979 to 2018 from station data. The new SCD for North America (SCDNA) includes daily precipitation, minimum temperature (T_{\min}), and maximum temperature (T_{\max}) data for ~~27280~~27276 stations. Raw meteorological station data were obtained from the Global Historical Climate Network Daily (GHCN-D), the Global Surface Summary of the Day (GSOD), Environment and Climate Change Canada (ECCC), and a compiled station database in Mexico. Stations with at least 8-year records were selected, which underwent location correction and were subjected to strict quality control. Outputs from three reanalysis products (ERA5, JRA-55, and MERRA-2) provided auxiliary information to estimate station records ~~and were also used as an assessment benchmark~~. Infilling during the observation period and reconstruction beyond the observation period were accomplished by combining estimates from 16 strategies (variants of quantile mapping, spatial interpolation, and machine learning). A sensitivity experiment was conducted by assuming 30% observations of stations were missing – this enabled independent validation and provided a reference for reconstruction. Quantile mapping and mean-value corrections were applied to the final estimates. The median Kling-Gupta efficiency (KGE') values of the final SCDNA for all stations are 0.90, 0.98, and 0.99 for precipitation, T_{\min} and T_{\max} , respectively. The SCDNA is closer to station observations than four benchmark gridded product, and can be used in applications that require either quality-controlled meteorological station observations or reconstructed long-term estimates for analysis and modelling. The dataset is available at <https://doi.org/10.5281/zenodo.3735533> ~~<https://doi.org/10.5281/zenodo.3735534>~~ (Tang et al., 2020).

209 **Key words:** serially complete dataset; precipitation; temperature; North America

210 **1 Introduction**

211 Station-based serially complete datasets (SCDs, see Table A1 for all acronyms) are important for meteorological,
212 climatological and hydrological studies (Kanda et al., 2018; Ramos-Calzado et al., 2008), such as ~~the production~~
213 ~~of producing~~ retrospective gridded products (Di Luzio et al., 2008; Kenawy et al., 2013; Newman et al., 2019; Serrano-
214 Notivoli et al., 2019), trend analysis (Knowles et al., 2006; Anderson et al., 2009; Papalexiou and Montanari, 2019),
215 and climatologic index calculation (Alexander et al., 2006; Papalexiou et al., 2018). These SCDs are useful because
216 station-based observational datasets often contain missing values due to factors such as observer absence, instrumenta~~l~~
217 failures and interrupted communication (Hasanpour Kashani and Dinpashoh, 2012). Moreover, station observations
218 failing quality control tests such as outlier and homogeneity checks may not be reliable (Menne et al., 2012), and many
219 stations are only maintained over a relatively short period of time or portions of the year, resulting in data gaps that
220 could affect the analysis of climate variability or long-term trends (Rubin, 1976; Stooksbury et al., 1999). Serial
221 completeness is also a critical requirement for real-time station-based applications, which regularly contend with
222 missing data values due to latencies in station reporting, quality control and processing (Tang et al., 2009).

223 Many methods have been developed to estimate missing observations and reconstruct time series of meteorological
224 stations that provide point-scale regular observations of atmospheric conditions.; ~~T~~hey can be ~~grouped-classified in~~
225 as self-contained infilling, spatial interpolation, quantile mapping ~~(QM)~~, and machine learning methods.

226 1. Self-contained infilling only uses records ~~of from~~ the target station to estimate its own missing values. Typical
227 methods include interpolation based on data from previous and subsequent days or replacing missing values by
228 long-term mean (Kemp et al., 1983; Pappas et al., 2014). Self-contained infilling, however, only performs well for
229 variables with high temporal autocorrelation such as temperature and is problematic for daily precipitation (Simolo
230 et al., 2010; Teegavarapu and Chandramouli, 2005), and in covering lengthy data gaps.

231 2. Spatial interpolation uses neighboring stations (identified on spatial distance or statistical similarity) to estimate data
232 at the target station. Spatial interpolation methods, ~~which~~ can be divided into two types: the first uses information
233 only from neighboring stations; and common methods include linear interpolation and inverse distance weighting
234 (IDW; Shepard, 1968). The second method needs information from both neighboring and target stations. Typical
235 examples include the revised normal ratio (NR; Young, 1992) and the single best estimator (Eischeid et al., 1995,
236 2000), both of which use correlation coefficients (CCs) between target and neighboring stations to estimate merging
237 weights. This second type of spatial interpolation also includes more sophisticated methods (e.g., multiple linear
238 regression, optimal interpolation, and kriging) that build a functional relationship between neighboring and target
239 stations (Simolo et al., 2010). Previous studies have shown that multiple linear regression based on the least absolute
240 deviation criteria (MLAD) performs better than many interpolation methods such as IDW, NR, and optimal
241 interpolation in infilling/reconstruction (Eischeid et al., 2000; Kanda et al., 2018).

242 3. Quantile mapping (QM) is widely used to correct biases ~~of in~~ meteorological data (Maraun, 2013; Cannon et al.,
243 2015) and performs well in estimating missing station data (Simolo et al., 2010; Newman et al., 2015, 2019; Devi
244 et al., 2019). In QM-based estimation, the cumulative distribution functions (CDFs) of observations from
245 neighboring and target stations are derived, and the record at the target station is estimated as the inverse of its CDF
246 using concurrent CDF probability information from neighboring stations. QM can avoid the problem of
247 overestimating wet days in precipitation series and preserve the frequency distribution of time series, which is useful
248 for estimating extreme events (Cannon et al., 2015).

249 4. Machine learning techniques have been successfully applied to infill station record gaps (Dastorani et al., 2010;
250 Wambua et al., 2016). For example, Coulibaly and Evora (2007) estimated missing daily precipitation and
251 temperature in northeastern Canada using six types of artificial neural networks (ANNs). Ustaoglu et al. (2008)
252 estimated daily temperature using three ANN methods in the Geyve and Sakarya basin, Turkey. Gene expression
253 programming was applied in the estimation of missing monthly rainfall data in Malaysia (Che Ghani et al., 2014).
254 Sattari et al. (2017) recommended that a decision-tree algorithm can be used to estimate monthly precipitation due
255 to its simplicity and high accuracy. Serrano-Notivoli et al. (2019) applied the k -nearest neighbours regression to
256 reconstruct minimum temperature (T_{\min}) and maximum temperature (T_{\max}) observations in Spain to form a gridded
257 dataset.

258 Previous SCDs have been developed using multiple infilling and reconstruction methods. For instance, Eischeid et al.
259 (2000) produced a daily SCD from 1951 to 1991 for the western United States (U.S.), including 2962 precipitation
260 stations and 2034 temperature stations; Vicente-Serrano et al. (2003) produced a daily SCD from 1901 to 2002 for
261 northeast Spain using 3106 precipitation stations; Di Piazza et al. (2011) built a monthly SCD from 1921 to 2004 for
262 Sicily, Italy using 247 precipitation stations; and Woldeesenbet et al. (2017) produced a daily SCD of precipitation and
263 temperature from 1980 to 2013 for the Upper Blue Nile Basin using six stations. There is currently no SCD for North
264 America; this means that researchers often must collect station data from different databases, which is time-consuming
265 and may cause inconsistencies between studies based on different methods.

266 Responding to this need, we develop a retrospective 40-year daily SCD for North America (SCDNA) of precipitation,
267 T_{\min} and T_{\max} from 1979 to 2018. Central America and Caribbean are also covered by SCDNA. The three variables
268 are selected because (1) most stations measure precipitation and temperature, while other variables, such as humidity
269 and wind speed are measured at fewer stations, and (2) precipitation and temperature data are fundamental inputs for
270 hydrological modeling. -Station observations are collected from four global and regional databases and undergo strict
271 quality control to eliminate dubious records. Since the performance of infilling and reconstruction methods differs in
272 space and time, the results from 16 strategies are merged to produce a single deterministic estimate. Finally, the
273 SCDNA is compared to four gridded products to demonstrate its performance and areas for improvement. The SCDNA
274 is expected to have a wide variety of applications in North America, and the methodology can be used to produce
275 SCDs in other regions of the world.

276 2 Datasets

277 2.1 Meteorological station data

278 This study uses precipitation, T_{\min} , and T_{\max} station data from four databases, the Global Historical Climate Network
279 Daily (GHCN-D; <https://www.ncdc.noaa.gov/ghcnd-data-access>; Menne et al., 2012), the Global Surface Summary
280 of the Day (GSOD; <https://catalog.data.gov/dataset/global-surface-summary-of-the-day-gsod>), Environment and
281 Climate Change Canada (ECCC; https://climate.weather.gc.ca/historical_data/search_historic_data_e.html), and the
282 Mexico database from Servicio Meteorológico Nacional, under the Comisión Nacional del Agua (Livneh et al., 2015).
283 This study uses daily precipitation totals from each dataset. Only stations with at least 8-year precipitation or T_{\min} and
284 T_{\max} records between 1979 to 2018 are utilized. The requirement for minimum recording length is different among
285 studies (e.g., Eischeid et al., 2000; Newman et al., 2015). We adopted a relatively short time limitation because (1) 8-
286 year records are sufficient to provide basic support for missing value estimation (Fig. S1), and (2) the open-access
287 dataset and codes enable users to design customized data selection criteria according to their research requirements.

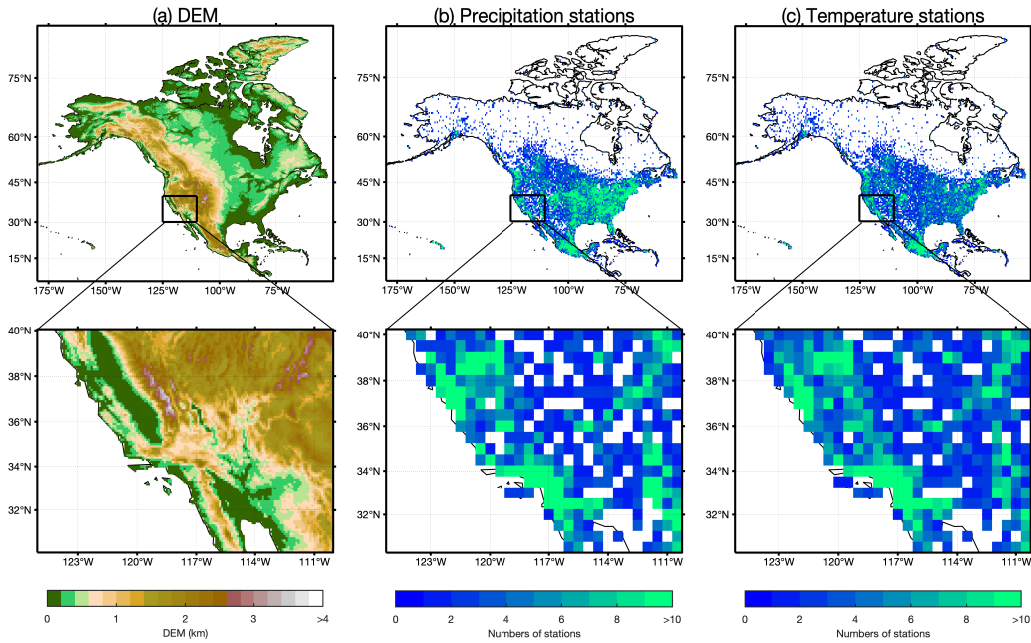
288 The numbers of stations with at least 8-year records are 33026, 4619, 3634, and 4049 for GHCN-D, GSOD, ECCC,
289 and the Mexico database, respectively (Table 1). Their spatial distributions are shown in Fig. S2. GHCN-D has
290 compiled a large amount of data from many sources including the Mexico database and ECCC. For identical stations
291 from different sources, we keep the one with longer observation history, resulting in the exclusion of ~95% of stations
292 from the Mexico database and adoption of ~91% of stations from ECCC. Stations with more than 30% missing values
293 in the observation period are excluded because they could be seasonal stations or suffer serious instrumentation
294 problems. Stations overlapping in space (same latitude and longitude) and without sufficient metadata for
295 discrimination are merged (see Sect. 3.2). The above screening reduces the available stations from 45328 to 31772
296 (Table 1), yet more stations are discarded due to quality control procedures (Sect. 3.1). The final SCDNA includes
297 24615 ~~24721~~ precipitation, 19677 ~~19604~~ T_{\min} , and 19684 ~~19611~~ T_{\max} stations; note that the numbers of T_{\min} and T_{\max}
298 stations differ as quality controls can result in excluding the one and reserving the other in some stations.

299 Most stations are located in the Contiguous United States (CONUS), southern Canada, and Mexico, while few stations
300 are located in high-latitude regions such as the Arctic Archipelago (Fig. 1b and c). The spatial distributions of
301 precipitation and temperature stations are similar, except in eastern CONUS where precipitation stations have a higher
302 density.

303 Table 1. Numbers of stations with at least 8-year records from 1979 to 2018

Station numbers	GHCN-D	GSOD	ECCC	Mexico	Merge	Total
Original numbers	33026	4619	3634	4049	0	45328
SCDNA input	24765	4331	3100	187	207	31772
SCDNA output: precipitation	19255	2656 <u>2551</u>	2440	170	200 <u>199</u>	24721 <u>24615</u>
SCDNA output: T_{\min}	13445 <u>13394</u>	3650 <u>3631</u>	2219	1671 <u>166</u>	1946	1960 <u>477</u>

304 Notification: “Merge” is derived from stations with overlapped locations from all the other data sources (Sect. 3.1.1).



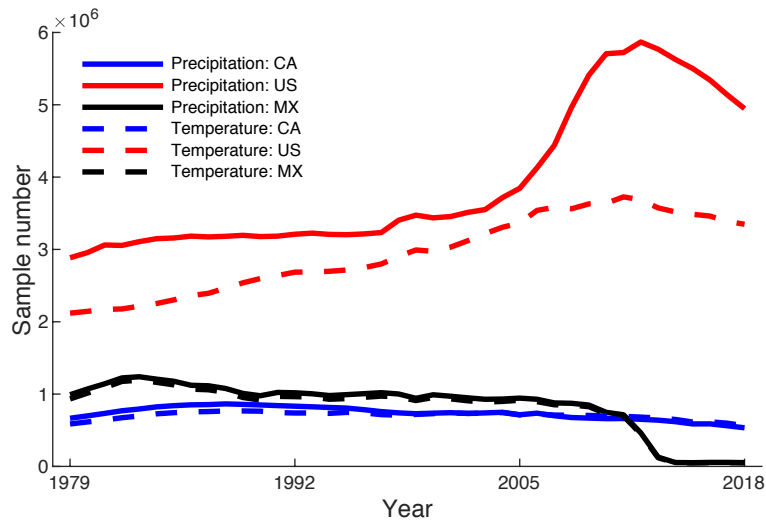
305

306 Figure 1. (a) Digital elevation model (DEM; Sect. 2.3) of North America. (b) and (c) are the densities of stations at
 307 the $0.5^\circ \times 0.5^\circ$ resolution for precipitation and temperature, respectively. T_{\min} and T_{\max} stations are highly consistent,
 308 and thus T_{\min} is used to represent temperature in (c). The nested black boxes show examples of DEM and station
 309 densities.

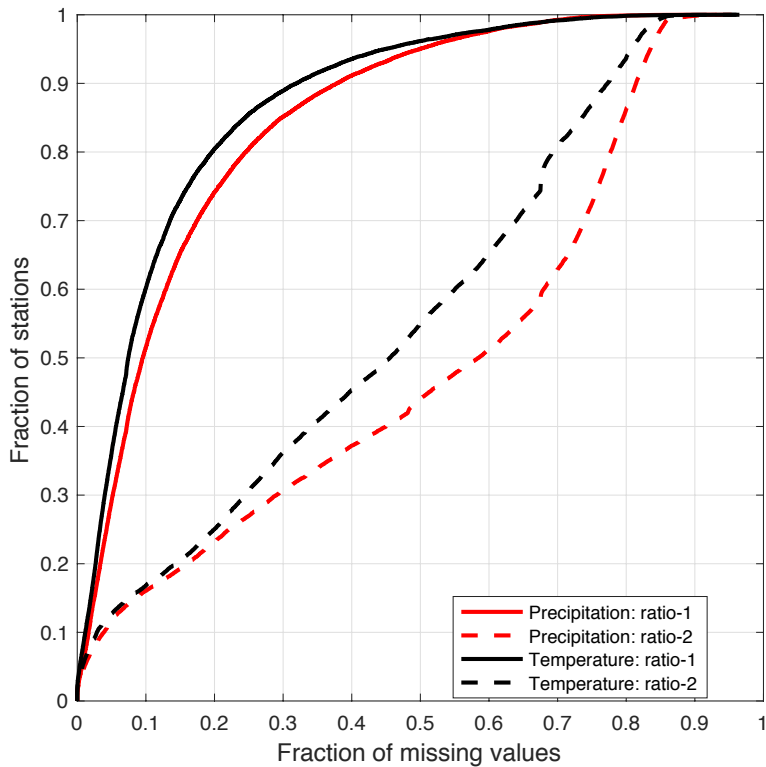
310 In North America, more station observations occur in U.S. than in Canada and Mexico (Fig. 2). The number of samples
 311 in U.S. increases from 1979 to 2018, and there are more precipitation samples than temperature samples. For Canada,
 312 the numbers of precipitation and temperature samples are similar and show a decrease from 1988 to 2018; the sample
 313 number in 2018 is only 61.76% of that in 1988. Mexico has more meteorological samples than Canada, yet this number
 314 decreases after 1983. The decreasing trend is especially sharp after 2012 which may be due to the delay in data
 315 collection or termination of some stations.

316 Figure 3 shows the fractions of missing values for all stations during the observation period (referred as ratio-1) and
 317 during the entire period from 1979 to 2018 (referred as ratio-2). For temperature, $\sim 20\%$ of the stations have more than
 318 20% missing values in the observation period (ratio-1), and $\sim 20\%$ of the stations have more than 70% missing values
 319 in the entire period (ratio-2). For precipitation, the fraction of missing values is larger. The fractions show strong
 320 spatial variations (Fig. S3). Ratio-2 is smaller for precipitation stations in western U.S. and temperature stations in
 321 central U.S., but larger in Canada and Alaska. Most stations in Mexico have higher ratio-1 than other regions in North
 322 America, indicating that those stations have notable fractions of missing values during the observation period.

323 In summary, the curves of ratio-1 indicate that a small number of missing values need infilling during the observation
 324 period, while the curves of ratio-2 indicate that extensive reconstruction is needed over the entire period.



325
 326 Figure 2. Sample numbers of stations for each year from 1979 to 2018. CA represents Canada, US represents United
 327 States, and MX represents Mexico. T_{max} stations are highly consistent with T_{min} stations, and thus T_{min} is used to
 328 represent temperature. The numbers of samples could be a better indicator than the numbers of stations because many
 329 stations have notable missing values.



330

331 Figure 3. The fraction of missing values for stations with at least 8-year records. Ratio-1 is the degree of missingness
 332 during the observation period, and ratio-2 is the degree of missingness during the entire period of interest (1979 to
 333 2018). T_{\min} is used to represent temperature because T_{\max} show almost overlapped curves with T_{\min} .

334 Many types of precipitation and temperature measurement instruments are used at stations from different sources. For
 335 example, the Type-B rain gauge is used by Environment Canada since 1970s for most weather stations (Devine and
 336 Mekis, 2008; Wang et al., 2017), while tipping bucket and weighing rain gauges are also used in some stations
 337 (Metcalfé et al., 1997). Nipher-shielded snow gauges have been used by some synoptic stations, while ruler
 338 measurements are still used by more stations (Mekis and Brown, 2010). Station data in U.S. are from many
 339 organizations or programs with different instrument configurations. For instance, the standard rain gauge is used by
 340 the Cooperative Observer Program while Snow Telemetry uses storage-type gauges or tipping buckets. A better
 341 understanding of instrument specifications and historical changes is important for climate studies (Pielke Sr et al.,
 342 2007; Whitfield, 2014; Ma et al., 2019). A detailed summary of station instruments is provided in the documentation
 343 of the dataset (<https://doi.org/10.5281/zenodo.3735533>).

344 2.2 Reanalysis products

345 We use reanalysis precipitation, T_{\min} and T_{\max} from the fifth generation of European Centre for Medium-Range
 346 Weather Forecasts (ECMWF) atmospheric reanalyses of the global climate (ERA5; Copernicus Climate Change
 347 Service (C3S), 2017), the Japanese 55-year Reanalysis (JRA-55; Kobayashi et al., 2015), and the Modern-Era
 348 Retrospective analysis for Research and Applications, Version 2 (MERRA-2; Gelaro et al., 2017) (see Table 2). The
 349 three products are chosen because they are representative products from different international organizations and they
 350 or their predecessor (ERA-Interim, JRA-25, and MERRA) have been widely used by researchers. The ERA5 and
 351 JRA-55 do not provide daily outputs, thus, daily precipitation is accumulated from sub-daily estimates while daily
 352 T_{\min} and T_{\max} are estimated by the sub-daily minimum and maximum temperature values. Gridded reanalysis
 353 precipitation is linearly interpolated to match point-scale station data, and T_{\min} and T_{\max} are downscaled using
 354 temperature lapse rate (TLR; see Sect. 3.1).

355 Table 2. Information on the three reanalysis products.

Products	Spatial resolution	Temporal resolution	Period	Agency
ERA5	0.25°×0.25°	1 h	1979-present	European Centre for Medium-Range Weather Forecasts
JRA-55	~5560 km	3 h	1958-present	Japan Meteorological Agency
MERRA-2*	0.5°×0.625°	daily	1980-present	NASA's Global Modeling and Assimilation Office

356 * MERRA-2 provides outputs in temporal resolutions from 1 h to 1 month; here we use daily values.

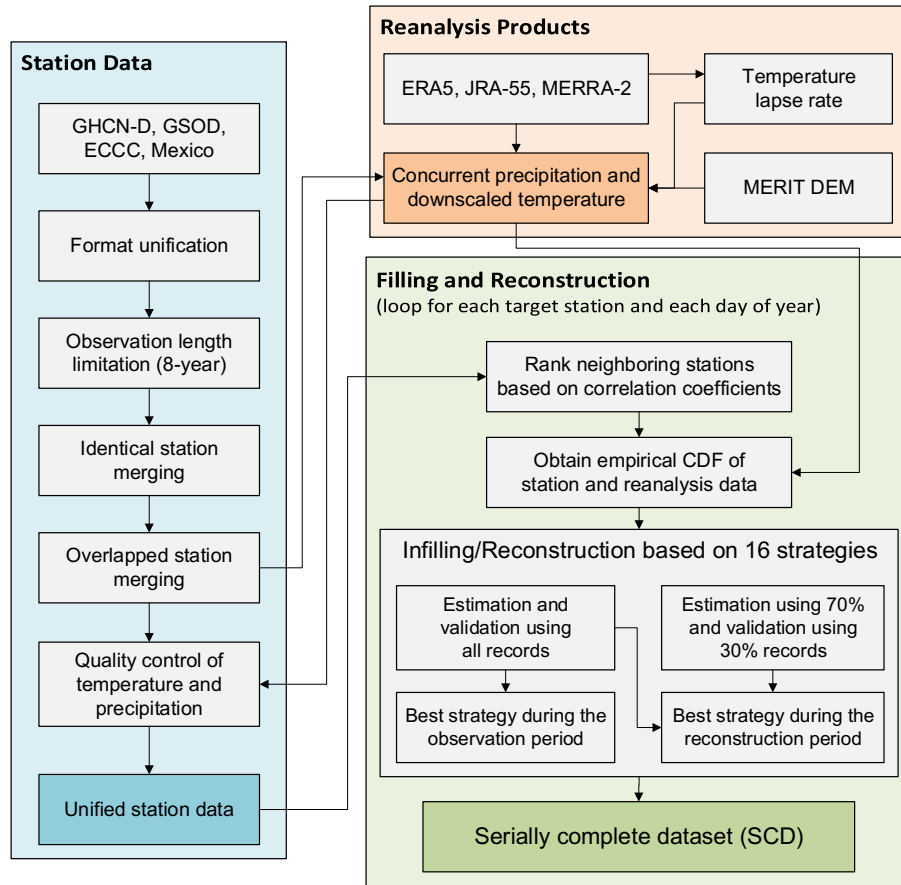
357 **2.3 Auxiliary data**

358 The Multi-Error-Removed Improved-Terrain digital elevation model (MERIT DEM) at a 3 sec (~90 m at the equator)
359 resolution (Yamazaki et al., 2017) is used in this study. To enable temperature downscaling, the high-resolution DEM
360 is spatially averaged to the original resolutions of ERA5, MERRA-2, and JRA-55 (Table 2). The MERIT DEM may
361 be slightly different than the DEM data used in the three reanalysis products, and this will have a limited impact on
362 missing data estimation (Sect. 3.3.2).

363 The Multi-Source Weighted-Ensemble Precipitation (MSWEP) V2.2 dataset (Beck et al., 2017, 2019) is utilized for
364 the comparison with the SCDNA developed by this study. MSWEP merges data from ground observations, satellite
365 products, and reanalysis models, and performs better than all products used for merging (Beck et al., 2019). The
366 comparison can show whether the SCDNA is a better choice than MSWEP to fill gaps in station precipitation
367 observations.

368 **3 Methodology**

369 The methodology to produce the SCDNA includes three primary steps (Fig. 4): (1) preparing a unified precipitation
370 and temperature database from multiple sources (Sect. 2.1 and 3.1); (2) downscaling reanalysis estimates (Sect. 2.2
371 and 3.2) that are used in QM- and machine learning-based data estimation (Sect. 3.3) and comparison with the SCDNA
372 (Sect. 4.5); and (3) producing the SCDNA from 1979 to 2018 based on 16 strategies (Sect. 3.3). The following sub-
373 sections summarize the work in each step of the methodology (Sect. 3.1, 3.2, and 3.3) as well as the approach used to
374 evaluate the performance of the method (Sect. 3.4).



375

376 Figure 4. Flowchart of the production of the SCDNA, including station data preparation, reanalysis product processing,
 377 and missing data infilling and reconstruction.

378 In this study, infilling refers to the estimation of missing values during the observation period, while reconstruction
 379 refers to estimating values outside of the observation period when no station record is available (Fig. 5). Station records
 380 that fail quality control are treated as missing values.

381 3.1 Prepare a unified precipitation and temperature database

382 3.1.1 Merging of stations based on location

383 Stations are merged if their latitude and longitude match other stations. The problem of overlapped locations is caused
 384 by identification alteration of one station for different periods, ~~or~~ recording/rounding bias of station location
 385 information, inconsistent naming rules of different sources, and other factors. Although it is possible that multiple
 386 stations are deployed in the same location for experimental aims, location merging is done to preserve internal
 387 consistencies as inconsistent records at the same location are self-contradictory.

388 The method for location merging includes several steps. First, overlapping stations are extracted and grouped. Stations
 389 within the same group that have non-overlapping recording periods are simply merged into one time series. Otherwise,

390 the Spearman's rank CC (SCC) between precipitation series from all station pairs in the group is calculated. For SCC
391 < 0.7 , the station group is discarded due to large discrepancies; for $0.7 < SCC < 0.9$ the discrepancy is considered as
392 tolerable and the station with the longest record is kept; for $SCC > 0.9$ stations are considered as highly correlated and
393 their data are merged into one time series, while for overlapping periods the station with longest record is used.

394 Overall, 1240 stations are involved in location merging, stratified in 586 station groups. Around 10% of the groups
395 contain more than two stations and the largest group contains five stations. After location merging, only 207 groups
396 are kept and merged into unified times series (Table 1). Despite the steps taken above, the merged series could contain
397 inhomogeneities due to the combination of records from multiple stations.

398 3.1.2 Quality control

399 To ensure station observations undergo strict and comprehensive quality control, we adopted the methods used to
400 produce previous station-based datasets. For T_{\min} and T_{\max} , we followed the method designed by Durre et al. (2010)
401 which is adopted by GHCN-D (Menne et al., 2012). The procedures include five types of checks: integrity checks,
402 outlier checks, internal and temporal consistency checks, spatial consistency checks, and extreme megaconsistency
403 checks. A few of the procedures in Durre et al. (2010) require other variables such as snowfall, and thus are not
404 adopted in this study. In addition, the quality flags in this study are partly different with those of GHCN-D because of
405 the different sources, numbers and temporal periods of stations.

406 For precipitation, quality control procedures consist of three parts. The first part is similar with that for temperature.
407 The second part (four types of checks) follows procedures designed by Hamada et al. (2011) which are adopted by
408 the Asian Precipitation-Highly-Resolved Observational Data Integration Towards Evaluation (APHRODITE; Yatagai
409 et al., 2012). The third part (two types of checks) adopts strategies by Beck et al. (2019) used in the production of
410 MSWEP. Note that although Durre et al. (2010) and Hamada et al. (2011) share some common traits for precipitation,
411 both of them are adopted to ensure quality control reliability.

412 ~~Details~~ The details of quality checks are in Appendix B.

413 3.2 Downscale reanalysis data

414 The reanalysis temperature estimates are downscaled to match point-scale station observations using temperature lapse
415 rate (TLR) according to

$$T_s = T_R + \text{TLR} \times \Delta h \quad (1)$$

416 where T_R is 2-m reanalysis air temperature, T_s is downscaled temperature, Δh is the height difference between station
417 elevation and reanalysis grid elevation. TLR shows notable spatiotemporal variations (Minder et al., 2010) and
418 estimating TLR based on ground observations over a large domain is difficult due to the sparsity of stations. Yet recent
419 studies show that reanalysis outputs offer an alternative in estimating gridded TLR (e.g., Gao et al., 2012). The gradient
420 of air temperature at different pressure levels above the ground can be used to approximate near-surface TLR (Gao et

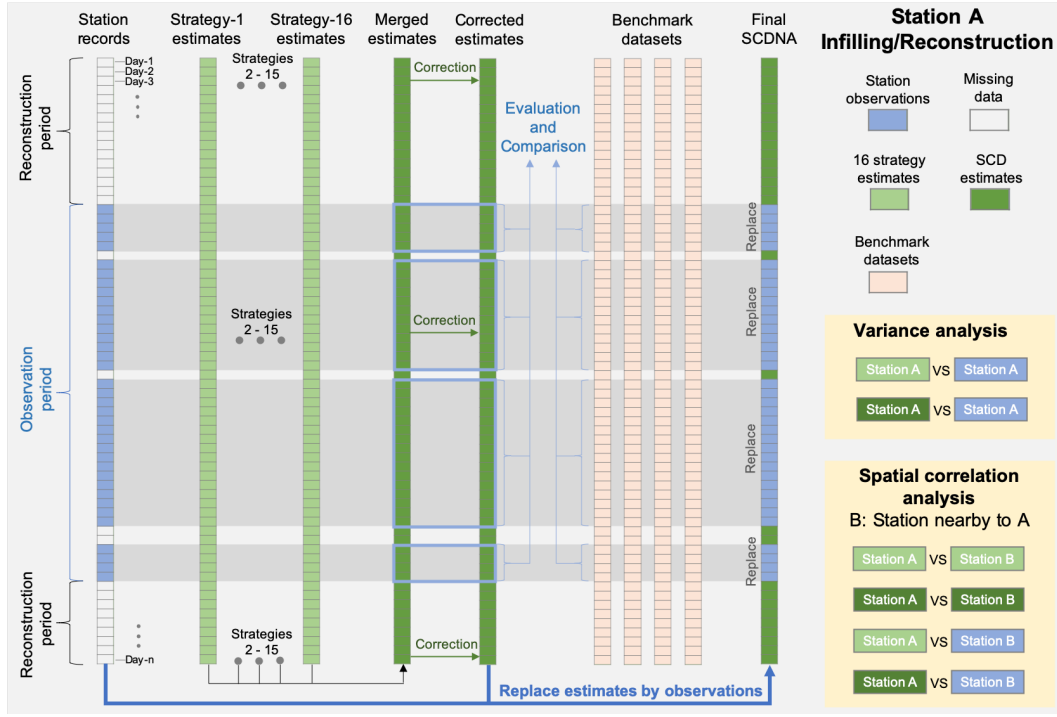
421 al., 2012, 2018; Gruber, 2012). Tang et al. (2018) compared eight temperature downscaling methods in CONUS and
422 found that methods based on reanalysis-derived TLR can achieve higher accuracy compared to fixed TLR (e.g., -
423 6.5°C/km) or statistical interpolation downscaling methods. Hence, this study uses the linear regression slope between
424 MERRA-2 air temperature and geopotential heights from 300 hPa to 1000 hPa pressure levels to represent TLR for
425 each month at the resolution of 0.5°×0.625° (Table 2). MERRA-2 is used because it directly provides monthly data
426 and masks temperature data if the pressure level is below land surface. The choice of pressure levels needs further
427 investigation because relationships between vertical and near-surface temperature vary with regions. Complicated
428 TLR phenomena such as inverse lapse rate are not considered for simplicity. The climatological mean of TLR (Fig.
429 S4) decreases from -4.8°C/km in the northeast continent (i.e., Canadian Arctic Archipelago) to -7.2°C/km in the
430 southwest continent (i.e., Rocky Mountains in CONUS). The smaller TLR magnitude in high latitudes is consistent
431 with previous studies (e.g., Gardner et al., 2009; Marshall et al., 2007).

432 **3.3 Produce the serially complete dataset**

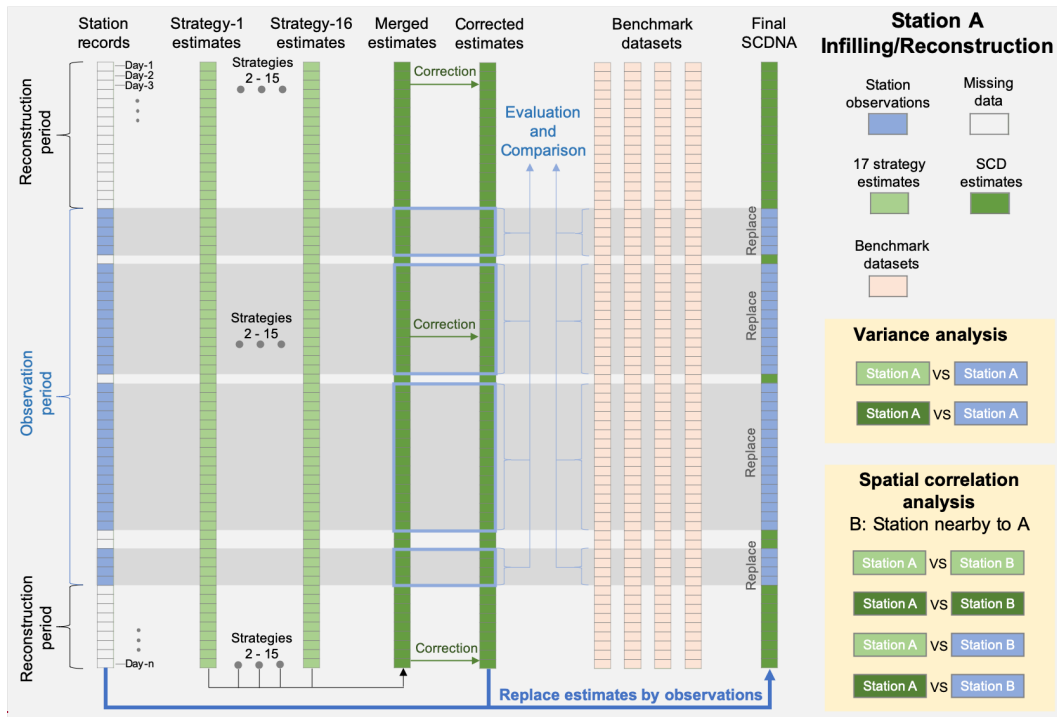
433 To produce the high-quality SCDNA for North America, we use 16 strategies: four based on quantile mapping with
434 neighboring stations (QMN; e.g., Longman et al., 2019; Newman et al., 2015, 2019), four on quantile mapping with
435 concurrent reanalysis estimates (QMR), four using spatial interpolation methods (INT; e.g., Eischeid et al., 2000;
436 Kanda et al., 2018; Woldesenbet et al., 2017), two using machine learning methods (MAL; e.g., Dastorani et al., 2010;
437 Wambua et al., 2016), and two multi-strategy merging methods (MRG). Merging multiple infilling/reconstruction
438 methods can provide better estimation than individual methods, as shown by previous data merging and gap infilling
439 studies (e.g., Eischeid et al., 2000; Beck et al., 2017, 2019; Ma et al., 2018).

440 We generate estimates for every station and every day from 1979 to 2018 (Fig. 5). The estimates from these 16
441 strategies and the SCDNA are evaluated using station observations, and the performance of the SCDNA is compared
442 to four benchmark gridded products. Then, the estimates of the SCDNA are corrected for further accuracy
443 improvement. Finally, estimates are replaced by station observations when observations exist and pass quality control
444 checks. The variance and spatial correlation analyses are performed to compare the statistical properties of station
445 observations and estimates (see Sect. 4).

446



447



448 Figure 5. Diagram of the infilling and reconstruction for a specific station (referred to as A). The entire period from
 449 1979 to 2018 is divided into the observation period and the reconstruction period. The data flows of variance and
 450 spatial correlation analyses are shown in the nested yellow boxes. Station B is a nearby station of A.

451 Only stations with at least 3000 valid values are included in the infilling and reconstruction effort. The ~~eight~~nine steps
 452 (termed Step-1 to Step-~~98~~) of SCDNA production are described as below. Unless otherwise stated, the steps are
 453 implemented for each target station (s), each variable (precipitation, T_{\min} , and T_{\max}), and each day of the year (DOY,
 454 i.e., 1-366).

455 3.3.1 Data extraction

456 **Step-1:** Spatiotemporally concurrent reanalysis estimates (ERA5, JRA-55, and MERRA-2) are extracted, including
 457 precipitation, T_{\min} , T_{\max} , and TLR. Precipitation is linearly interpolated from gridded reanalysis estimates, and
 458 temperature is downscaled (i.e., corrected for the elevation difference between the reanalysis grid cell and the station
 459 elevation) based on TLR (Sect. 3.1).

460 **Step-2:** Neighboring stations (at least one and at most 30) with at least 8-year overlapped period with station s are
 461 found within the searching radius of 200 km. These stations are ranked from closest to farthest according to their CC
 462 with the target station. SCC is used for precipitation, and Pearson CC (PCC) is used for T_{\min} and T_{\max} . CC is calculated
 463 using data within a 31-day window centered around the current DOY from all years.

464 **Step-3:** The empirical CDFs of s , neighboring stations, and reanalysis estimates are obtained using data within the
 465 same 31-day window.

466 3.3.2 Infilling and reconstruction

467 **Step-4:** For each day (d) corresponding to the DOY, the estimated data are acquired based on 16 strategies which are
 468 divided into five groups.

469 **Group 1: Quantile Mapping with Neighboring stations (QMN)**

470 • **QMN-1:** For all neighboring stations with valid records, the station with the highest CC in Step-2 is selected.
 471 The estimated data for s and d is obtained using Eq. (2).

$$X_s = F_s^{-1}(F_i(X_i)) \quad (2)$$

472 where X_i is precipitation or temperature for d from the selected neighboring station i , F_i is the empirical CDF of
 473 i corresponding to the DOY, F_s^{-1} is the inverse CDF of s corresponding to the DOY, and X_s is the estimated data.

474 • **QMN-2:** For all neighboring stations with observations, estimated values are obtained using Eq. (2) which are
 475 merged based on Eq. (3).

$$X_s = \frac{\sum_i^n W_i F_s^{-1}(F_i(X_i))}{\sum_i^n W_i} \quad (3)$$

$$W_i = CC_i^2 \quad (4)$$

476 where n is the number of neighboring stations, $F_s^{-1}(F_i(X_i))$ is the QM-based estimate from i , and W_i is the weight
 477 calculated using Eq. (4). CC_i is CC (SCC or PCC) between data from s and i corresponding to the DOY. W_i is
 478 assigned zero if CC_i is negative.

- 479 • **QMN-3:** Similar to QMN-2, but the weight is calculated according to the distance (D_i) between s and i based on
 480 Eq. (5). Although the exponent of distance (k) varies in different studies, -2 is the most common choice
 481 (Teegavarapu and Chandramouli, 2005).

$$W_i = D_i^k \quad (5)$$

- 482 • **QMN-4:** The median of QMN-1 to QMN-3 is used as the estimated data. The strategy of using median values is
 483 the same with Eischeid et al (2000), which could be closer to actual observations than QMN-1 to 3.

484 **Group 2: Quantile Mapping with Reanalysis products (QMR)**

485 Reanalysis products provide useful information for SCDNA production as (1) remote regions may not have enough
 486 neighboring stations, and (2) neighboring stations also have missing values which could result in gaps of estimates at
 487 the target station.

- 488 • **QMR-1 to QMR-3:** Similar to QMN-1, but the neighboring station is replaced by concurrent ERA5, JRA-55,
 489 and MERRA-2 estimates, respectively.
- 490 • **QMR-4:** The median of QMR-1 to 3 is used as the estimated data.

491 **Group 3: Interpolation (INT)**

492 The three interpolation methods used in this study are MLAD (referred as INT-1), NR (referred as INT-2), and inverse
 493 distance weighting (IDW, referred as INT-3). They are described below. Following Eischeid et al. (2000), neighboring
 494 stations with CC lower than 0.35 are excluded. The remaining stations are ranked from high CC to low CC. A
 495 maximum of four neighboring stations are used in the interpolation. For T_{\min} and T_{\max} , direct interpolation from
 496 neighboring stations to s could be biased due to the elevation differences between stations. Temperature data from
 497 neighboring stations are downscaled to the elevation of s based on Eq. (1).

- 498 • **INT-1:** MLAD minimizes the sum of absolute errors. It is more robust than regression based on least squares
 499 because while least square estimation is effective when the errors are normally distributed and independent,
 500 environmental variables, especially precipitation, often violate the assumption of normality (Eischeid et al.,
 501 2000). MLAD has been well documented with better performance in gap infilling than other interpolation
 502 methods (Eischeid et al., 1995, 2000; Kanda et al., 2018; Young, 1992). The formula is shown in Eq. (6).

$$X_s = c_0 + \sum_i^n c_i X_i \quad (6)$$

503 where c_i ($i=0, 1, \dots, n$) is regression coefficients estimated using data within a 31-day window for each DOY.
 504 Different d corresponding to the same DOY could have different combinations of neighboring stations due to the
 505 limitation of observation availability. MLAD is performed for each combination to ensure that effective estimates
 506 are available for all days.

- 507 • **INT-2:** NR is an interpolation method proposed by Paulhus and Kohler (1952) and modified by Young (1992).
 508 The modified version is adopted in this study, which combines information from neighboring stations by
 509 replacing $F_s^{-1}(F_i(X_i))$ with X_i in Eq. (3). The weight is calculated using Eq. (7).

$$W_i = CC_i^2 \frac{N_i - 2}{1 - CC_i^2} \quad (7)$$

510 where N_i is the number of samples used to calculate CC_i between s and i . SCC is used for precipitation and PCC
 511 is used for temperature.

- 512 • **INT-3:** IDW is one of the most common interpolation methods. It is implemented similar to NR, where the
 513 inverse squared distance, as shown in Eq. (5), is used as the weight.
- 514 • **INT-4:** The median of INT1, INT2 and INT3 is used as the estimated data.

515 **Group 4: Machine Learning (MAL)**

516 The two MAL methods used in this study are ANN (referred as MAL-1) and random forest (RF, referred as MAL-2;
 517 Breiman, 2001). Unlike QMN, QMR and INT that are carried out for each DOY, MAL uses complete observation
 518 records of s to ensure that ANN and RF are trained with enough values. MAL models are trained using the first 70%
 519 observations and tested using the remaining 30% observations. The MAL models' validation based on the 30%
 520 observations can indicate their performance in the reconstruction period.

521 The input data are from neighboring stations and concurrent reanalysis estimates. For each s , neighboring stations are
 522 determined in a way similar with Step-2, but CC is calculated using data in the entire observation period. Neighboring
 523 stations with CC lower than all reanalysis products (ERA5, JRA-55, and MERRA-2) are excluded. The remaining
 524 neighboring stations and three reanalysis products form a complete repository of input features. Then, for each day
 525 that s has no observation, the input features are extracted from the repository in three steps: (1) neighboring stations
 526 without observations for the day are excluded, (2) the remaining neighboring stations and reanalysis products are
 527 ranked according to their CC with s , and (3) at most five stations/reanalysis products with the highest CC are selected.
 528 In this way, s will have multiple combinations of input features to ensure that all days with missing values have
 529 estimates. All combinations are used to train and test the ANN and RF models, resulting in multiple estimated series

530 for s . The final estimates of s are generated in three steps: (1) the Kling-Gupta Efficiency (KGE'₁; Kling et al., 2012)
531 of all estimated series is calculated using all observations of s , and ranked from high to low KGE'₁ (see Sect. 3.4 for
532 definition of KGE'₁); (2) the series with higher KGE'₁ is used to constitute the estimates of s in sequence; and (3) the
533 second step is repeated until there are no missing values for s . This approach ensures that “best” and complete estimates
534 are provided for s .

535 • **MAL-1:** A four-layer ANN is used. The input layer has a maximum of five nodes (depending on the number of
536 input features), the two hidden layers both have 20 nodes, and the output layer has one node for generating
537 precipitation or temperature estimates. The transfer functions are hyperbolic tangent sigmoid for hidden layers
538 and linear for the output layer. The training function is resilient backpropagation. The model is trained using the
539 first 50% data, validated using the subsequent 20% data, and tested using the final 30% data.

540 • **MAL-2:** A RF model with 50 trees is built with 70% training data and 30% testing data. The minimum number
541 of samples per tree leaf is 5. The input nodes depend on the number of input features like MAL-1.

542 **Group 5: Multi-Strategy Merging (MRG)**

543 • **MRG-1:** KGE'₁ is used to rank the performance of the 11 strategies (QMN-1 to 3, QMR-1 to 3, INT-1 to 3,
544 and MAL-1 to 2) as CC cannot reflect the magnitude difference (e.g., bias) between target and reference
545 series. The first three cases of the 11 strategies are merged using squared KGE'₁ as the weight. The individual
546 weight is assigned zero if KGE'₁ is negative.

547 • **MRG-2:** The median of the three selected strategies in MRG-1 is used as the estimated data.

548 *3.3.3 Generating serially complete records*

549 **Step-5:** In this step, Step-3 and -4 are repeated based on 70% data of s in the observation period. Then, the KGE'₁ of
550 estimates from all strategies are calculated using the remaining 30% observations. MAL-1 and 2 are not repeated
551 because they are trained on the 70% observations. Although the evaluation samples are different among stations, the
552 results are reliable and stable as shown in the results section. This step is implemented because QMN-1 to 4, QMR-1
553 to 4, and INT-1 in Step-4 use all data of s in the observation period to select stations, estimate empirical CDFs and
554 carry out regression. This potential overfitting problem could lead to better performance of these strategies in the
555 observation period but worse performance in the reconstruction period. KGE'₁ calculated in Step-4 can represent the
556 accuracy of estimates in the observation period, while KGE'₁ calculated in Step-5 can represent the accuracy of
557 estimates in the reconstruction period.

558 **Step-6:** In the observation period, the strategy with the highest KGE'₁ in Step-4 is selected to contribute the
559 extension/reconstruction to the SCDNA. In the reconstruction period, first, the strategy with the highest KGE'₁ in Step-
560 5 is determined; then, the estimates from the corresponding strategy in Step-4 are used to constitute the SCDNA

561 because the empirical CDF and regression based on all observations in Step-4 could be more representative than the
 562 70% observations in Step-5.

563 **Step-7:** Estimates in Step-6 are corrected for certain climatological biases using station data in the observation period.
 564 Precipitation estimates are often subjected to wet-day bias. Two methods are implemented to address this problem.
 565 First, QM is performed based on the CDF of s in Step-3. However, QM may reduce the accuracy of estimated
 566 precipitation in some cases, for which the method used in Beck et al. (2019) is adopted. This method subtracts a tiny
 567 value (0.01 mm) from the original precipitation series and rescales the series to restore the original mean value. This
 568 operation is repeated until the estimated series show equal number of wet days ($>0.5 \text{ mm d}^{-1}$) with observations of s .
 569 In addition to wet-day bias correction, mean-value correction is implemented. The ratio between the mean values of
 570 precipitation estimates and observations is calculated in the observation period, which is used to rescale estimated
 571 series in both observation and reconstruction periods. For T_{\min} and T_{\max} , QM correction and mean-value correction are
 572 also implemented.

573 **Step-8:** The accuracy of the SCDNA is evaluated and compared to benchmark datasets based on actual observations
 574 (Fig. 5). Then, the estimates are replaced by observations whenever possible to generate the final SCDNA. Very
 575 occasionally, estimated T_{\min} could be larger than estimated T_{\max} , for which T_{\max} is replaced by the maximum T_{\max} , and
 576 T_{\min} is replaced by the minimum T_{\min} of the estimates from the 16 strategies.

577 **Step-9: The serially complete data of SCDNA is quality controlled again using methods introduced Sect. 3.1.2 to**
 578 **exclude stations with unreliable estimates.**

579 3.4 Evaluate the precipitation and temperature estimates

580 KGE'_s , which is proposed by Gupta et al. (2009) and modified by Kling et al. (2012), is used to support the merging
 581 of different strategies (Sect. 3.3) and the evaluation of the estimated precipitation and temperature. ~~It is a useful metric~~
 582 ~~in evaluating various variables (e.g., Tang et al., 2020) and incorporates information about correlation, bias, and~~
 583 ~~variance.~~

$$\begin{cases} KGE'_s = 1 - \sqrt{(r - 1)^2 + (\beta - 1)^2 + (\gamma - 1)^2} \\ \beta = \frac{\mu_s}{\mu_o} \\ \gamma = \frac{CV_s}{CV_o} = \frac{\sigma_s/\mu_s}{\sigma_o/\mu_o} \end{cases} \quad (8)$$

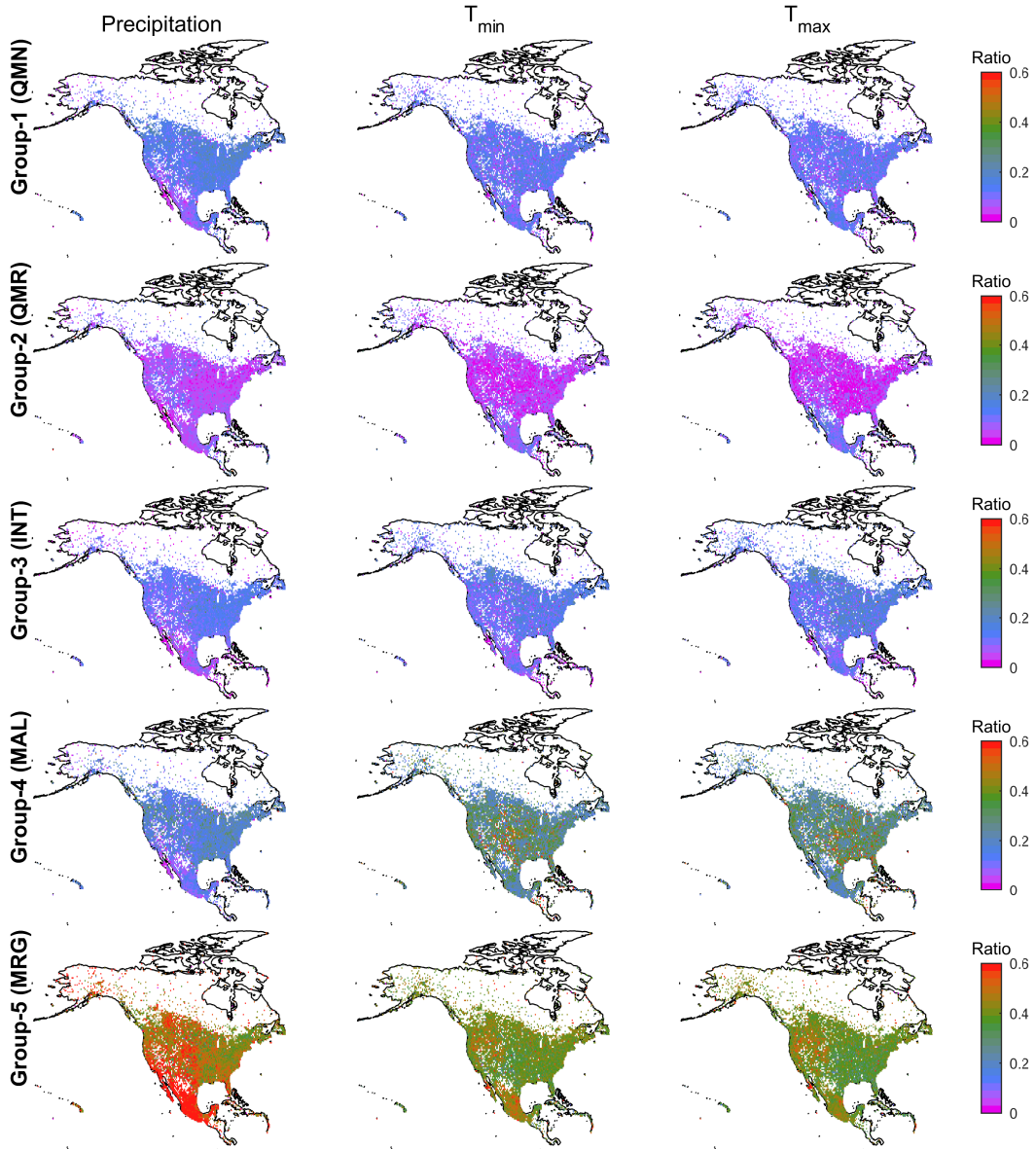
584 where r is the PCC, β is the bias ratio, and γ is the variability ratio; μ is the mean value, and σ is the standard
 585 deviation. The subscripts s and o represent estimated and reference time series, respectively. KGE'_s ranges from
 586 negative infinity to one. If two series exactly match, the KGE'_s is one. A β or γ value smaller/larger than one indicates
 587 that the mean value or variability of observations is underestimated/overestimated.

588 In Sect. 4, the evaluation during the observation period is based on the complete station observations (i.e., Step-4 in
589 Sect. 3.3.2), while the evaluation during the reconstruction period is realized using 30% independent station
590 observations (i.e., Step-5 in Sect. 3.3.3). Unless otherwise stated, SCDNA estimates in Sect. 4 are after correction
591 (Step-7 in Sect. 3.3.3). In Sect. 4.5, SCDNA estimates are compared with gridded products (ERA5, JRA-55, MERRA-
592 2, and MSWEP). In addition to the three SCDNA variables (precipitation, T_{\min} , and T_{\max}), mean temperature (T_{mean} ,
593 the mean of T_{\min} and T_{\max}) and daily temperature range (T_{range} , the difference between T_{\max} and T_{\min}) are also included.
594 The involvement of T_{range} can contribute to more objective comparison between SCDNA and reanalysis products
595 because the TLR-based downscaling of reanalysis temperature contains uncertainties, which could affect the
596 evaluation of T_{\min} , T_{\max} , and T_{mean} . Although there exist differences between TLR of T_{\min} and T_{\max} , T_{range} can reduce
597 the effect of scale-mismatch between gridded reanalysis temperature and point station temperature on evaluation
598 results.

599 **4 Results**

600 **4.1 Comparison of infilling and reconstruction strategies**

601 The value of a given infilling/reconstruction strategy can be quantified by the extent that a strategy is selected for use
602 in the final SCDNA dataset. In this sense the contribution ratios define the proportion of estimates that come from a
603 specific strategy. Fig. 6 shows that the contribution ratios of QMN, QMR, and INT to missing value estimation are
604 generally smaller than 20% in North America. Please note that QMN refers to all strategies within this group unless
605 the strategy number is specified right after QMN. This also applies to other groups. QMR shows the smallest
606 contribution ratios for almost all stations among the five groups. Compared with other regions in North America,
607 contribution ratios of QMR are higher for precipitation stations in western U.S. and temperature stations in Mexico.
608 INT shows lower contribution ratios in Rocky Mountains compared with western U.S., indicating statistical
609 interpolation without considering topographic effect is subjected to substantial uncertainties in complex terrain. MAL
610 shows notably higher contribution ratios than QMN, QMR, and INT, particularly for T_{\min} and T_{\max} . The ratios of MAL
611 are higher than 20% for ~30% precipitation stations, ~65% T_{\min} stations, and ~68% T_{\max} stations. MRG has the highest
612 contribution ratios throughout North America. The average contribution ratios of MRG are 59.88%, 41.59%, and
613 40.56% for precipitation, T_{\min} , and T_{\max} , respectively. For precipitation, MRG is particularly effective in high-latitude
614 regions (northern Canada and Alaska), western U.S. and Mexico.



615

616 Figure 6. The contribution ratios of estimates from five infilling/reconstruction groups to the missing values of all
 617 stations from 1979 to 2018. The three columns from left to right represent precipitation, T_{\min} , and T_{\max} , respectively.
 618 The five rows from top to bottom represent Group-1 (QMN), Group-2 (QMR), Group-3 (INT), Group-4 (MAL), and
 619 Group-5 (MRG), respectively. The maps are at the resolution of 0.5° . The ratio for each grid cell is the mean value of
 620 all stations within this grid cell.

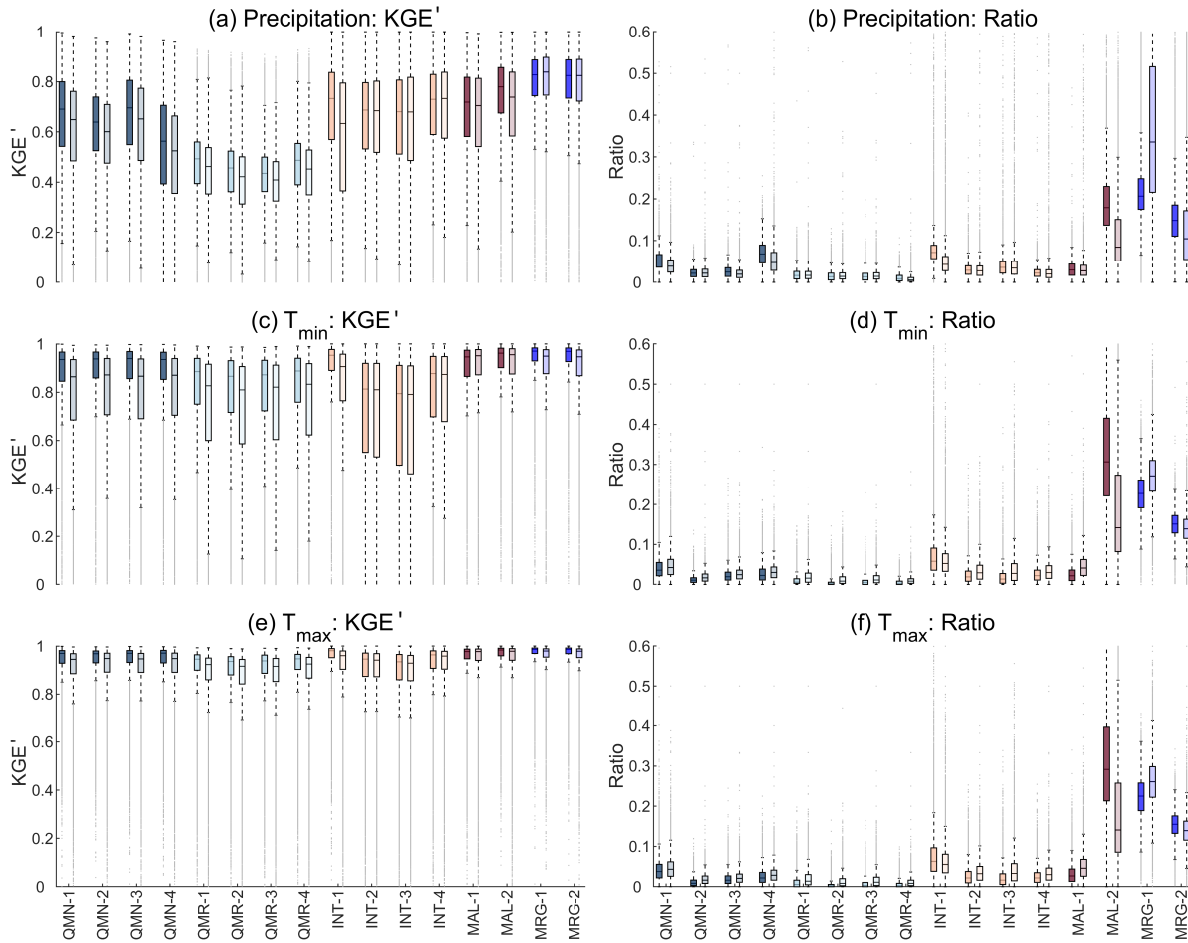
621 Figure 7 shows the KGE'_i and contribution ratios of 16 strategies. The KGE'_i of estimated precipitation is lower than
 622 that of estimated T_{\min} and T_{\max} due to the stronger spatial and temporal homogeneity of temperature (Fig. 7). The
 623 median KGE'_i values of T_{\min} and T_{\max} are generally above 0.9, and the accuracy of estimated T_{\max} is higher than that
 624 of T_{\min} . The KGE'_i during the reconstruction period is smaller than that during the observation period, which is

625 particularly obvious for QMN, QMR, and INT-1 compared with other strategies, because QMN and QMR transfer
626 CDF during the observation period to other periods, and INT-1 transfers regression relationship during the observation
627 period to other periods. MAL suffers a slight degradation in the reconstruction period, and the better performance of
628 MAL-2 than MAL-1 shows that RF could be a better choice than ANN in estimating missing data. For MRG, the
629 differences of KGE'_i between the two periods are relatively small. For example, the median KGE'_i values of MRG-1
630 for T_{max} are 0.99 and 0.98 for observation and reconstruction periods, respectively. MRG also shows higher KGE'_i and
631 a narrower quantile ranges than other strategies, particularly for precipitation, benefiting from merging estimates from
632 multiple strategies

633 Regarding contribution ratios (Fig. 7), strategies with higher KGE'_i often have larger contributions to the estimated
634 series. However, this is not always true because the selection of strategies is performed for each DOY. Note that the
635 contribution ratios of MAL-2 are even higher than MRG-1 during the observation period for T_{min} and T_{max} , although
636 MRG-1 achieves higher KGE'_i than MAL-2 for most stations. This is because MAL-2 could be the best choice for
637 more DOY than MRG-1 even though MRG-1 may achieve the best overall performance. An example using T_{min} data
638 from one station is shown in Fig. S5.

639 In the reconstruction period when observations are absent, the contribution ratios of MAL-2 decrease drastically
640 compared with the observation period, contributing to the increased ratios of other strategies (particularly MRG-1).
641 Although QMR shows the lowest contribution ratios, reanalysis products have implicit contributions to other strategies
642 (e.g., MAL and MRG). Overall, MRG-1 shows much higher contribution ratios than all the other strategies (including
643 MRG-2) during the reconstruction periods, indicating that it is the most important strategy in missing value estimation.
644 Hence, combining information from multiple strategies is more reliable, and KGE'_i -based merging is more effective
645 than the median-value-based estimation.

646



647

648 Figure 7. Boxplots of (a, c, and e) the KGE' and (b, d, and f) the contribution ratio of 16 strategies for all stations.
 649 Each strategy corresponds to two boxes in each sub-figure; the left one with darker color represents the observation
 650 period, and the right one with lighter color represents the reconstruction period. The line within the box is the median.
 651 The upper and lower edges of the box represent the 25th and 75th percentiles, respectively. Values more than 1.5
 652 times the interquartile range away from the upper or lower edges are outliers (dots).

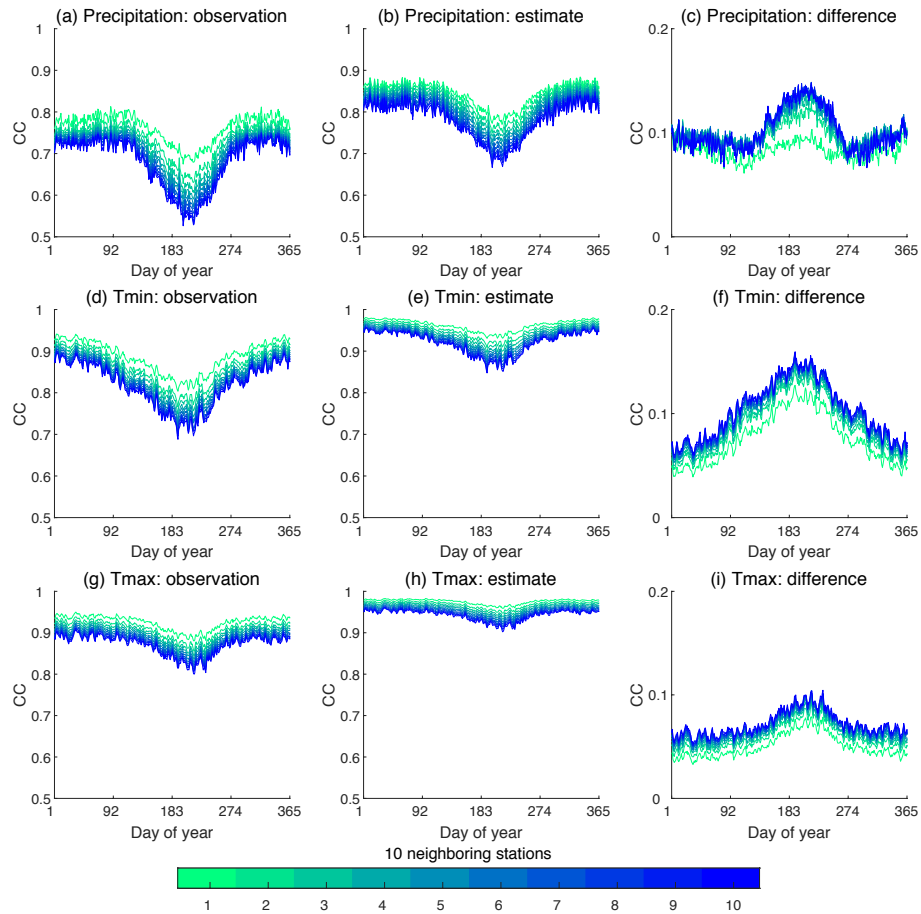
653 **4.2 Impact of reconstruction on spatial correlation and series variance**

654 All infilling/reconstruction strategies except QMR rely on information from neighboring stations; this could affect the
 655 spatial correlation structure and the variance of SCDNA series. Space-time correlations and other properties (e.g.,
 656 intermittency of precipitation) are important considerations because they can influence the performance of follow-on
 657 applications that use the SCDNA as input. Theoretically, QMN strategies could significantly inflate spatial correlation
 658 but retain variance of station observations. The spatial correlation inflation in INT strategies could be lower but the
 659 variance would be underestimated due to smoothing. QMR-1 is used as an example to demonstrate the effect of QM
 660 on spatial correlation and series variance (Fig. S6), because QMN uses different station combinations for every DOY
 661 which would mask the effect of QM on final estimates. If the ERA5 used by QMR-1 is replaced by station observations,
 662 the results should be generally consistent. According to Fig. S6, the spatial correlation is substantially inflated by

663 QMR-1, particularly for T_{\min} and T_{\max} , while the standard deviation of QMR-1 estimates is very close to that of
664 observations. This supports the design of estimating missing data using neighboring stations for each DOY as
665 otherwise the inflation of CC could be very substantial for the entire period.

666 The spatial correlation based on station observations (Fig. 8a, d, and g) shows obvious seasonal variations, with CC
667 lower in the warm season and higher in the cold season. The seasonality of CC for T_{\max} is weaker compared with that
668 for precipitation and T_{\min} . The SCDNA estimates capture the seasonal patterns but underestimates the variation (Fig.
669 8b, e, and h) because the inflation of spatial CC is larger in the warm season than cold season (Fig. 8c, f, and i).
670 Moreover, the inflation is larger for neighboring stations with lower correlation with the target station. We tested
671 selecting neighboring stations according to their distance from the target station, and similar results were acquired.
672 For precipitation, the median CC differences of all stations are close to 0.1 in the cold season and ranges between 0.1
673 and 0.15 in the warm season. For T_{\min} , the median CC differences are generally between 0.05 and 0.15. The CC
674 differences of T_{\max} are relatively homogeneous for different seasons and generally fluctuate between 0.05 and 0.1. The
675 inflation of CC is because (1) the estimates from the 10 neighboring stations and the target station are generally derived
676 using highly overlapped information (Sect. 3.3.1), and (2) estimation is realized for each DOY for all strategies except
677 MAL, meaning that calculating CC for each DOY show the inflation to the largest extent.

678 The final SCDNA replaces estimates by observations, which can largely relieve the inflation of spatial correlation
679 (Fig. S7), depending on the degree to which observations are present in the record. For T_{\min} and T_{\max} , CC is very close
680 to that based on observations; for precipitation, correlation in wintertime is even lower than that based on observations.



681

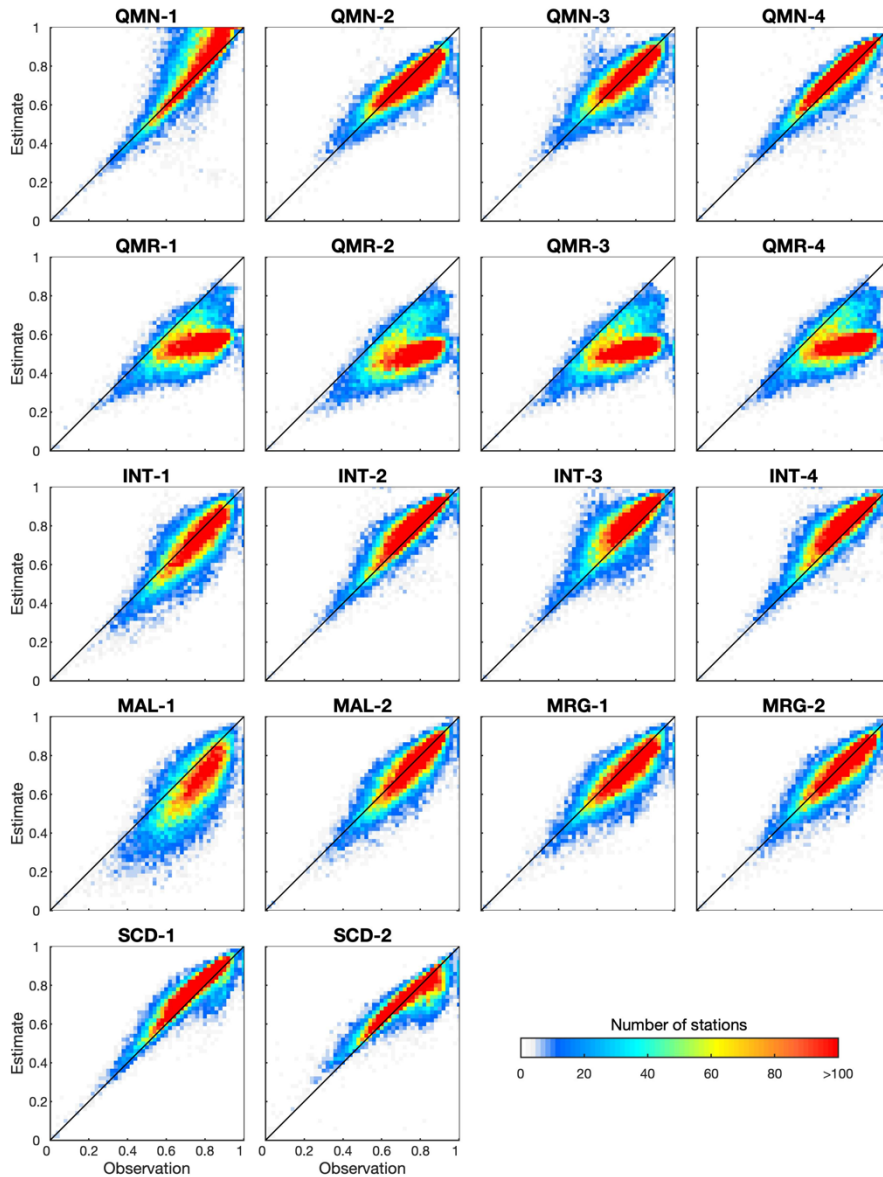
682 Figure 8. CC between target and neighboring stations for all DOY using station observations (the first column),
 683 SCDNA estimates (second column), and differences between SCDNA- and observation-based CC (the third column).
 684 CC is calculated in the observation period. For each target station, 10 neighboring stations are selected according to
 685 the correlation between time series from target and neighboring stations. Smaller numbers represent higher correlation.
 686 For example, station 1 represents the neighbor with the highest CC with the target station. Each curve represents the
 687 median CC of all stations.

688 Figures 9 and 10 show CC between estimates at the target station and observations at the neighboring station. For
 689 precipitation, most strategies exhibit similar spatial correlation structure with observations for most stations. QMR
 690 largely underestimates CC compared with observations, which should be attributed to the differences between
 691 precipitation of reanalysis products and stations. There are notable differences for different strategies within one group.
 692 For example, QMN-1 shows larger inflation when observation-based CC is higher, which is not seen in QMN-2 to 4.
 693 This is probably because QMN-1 only uses information from the one neighboring station with the highest correlation
 694 with the target station for each DOY. Higher observation-based CC in Fig. 9 means this neighboring station could be
 695 more frequently used by QMN-1 to estimate data for the target station, resulting in the larger inflation of CC. Another
 696 example is that INT-1 underestimates the CC for 68.75% stations, whereas INT-2 to 4 overestimates the CC for almost
 697 all stations. For SCD-1, inflation of CC is observed for 76.60% stations, whereas the magnitude of overestimation is

698 smaller than that in Fig. 8. The mean values of observation-based and estimate-based CC are 0.71 and 0.77,
699 respectively. SCD-2 replaces estimates by observations and is the final dataset of this study. It reduces the mean
700 estimate-based CC to 0.70. The overall spatial correlation structure of observations is generally preserved by SCD-2.
701 However, SCD-2 calculates CC for the entire period which is different from the period of observation-based CC,
702 resulting in uncertainties such as the underestimation for some stations when observation-based CC is larger than 0.7.

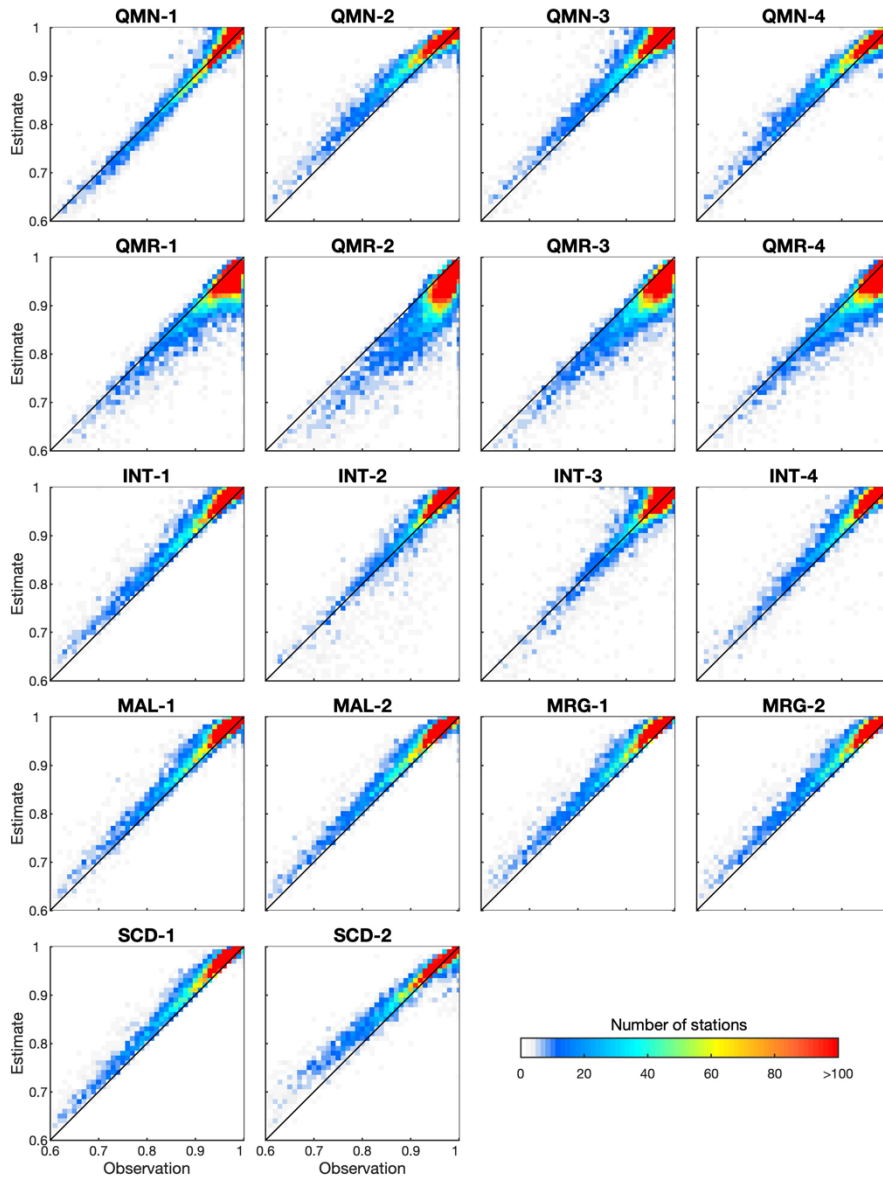
703 The spatial correlation of T_{\min} is much stronger than that of precipitation (Fig. 10). Most strategies overestimate the
704 CC for most stations, whereas the magnitude is quite small. For example, SCD-1 inflates the CC for 96.96% stations,
705 while the mean CC values for observations (0.95) and SCD-1 (0.96) are very close to each other. QMR still
706 underestimates CC similar to Fig. 9 for precipitation. CC based on SCD-2 is generally consistent with that based on
707 observations, while slight underestimation exists for some stations when observation-based CC is higher than 0.9. T_{\max}
708 shows similar spatial correlation patterns with T_{\min} (Fig. S8).

709 In summary, inflation of CC is inevitable particularly when estimates are obtained using information from sole data
710 source such as one neighboring station or one reanalysis product. The inflation is larger if each DOY is treated
711 separately (Fig. 8 and S7), but smaller if CC is calculated for all years (Fig. 9, 10 and S8). Combining information
712 from multiple sources (stations and reanalysis) and combining multiple strategies for each DOY are beneficial in
713 estimating the overall spatial correlation structure. The spatial correlation structures vary for different strategies, and
714 further studies are needed to clearly demonstrate how and why the estimate-based CC differs from observation-based
715 CC.



716

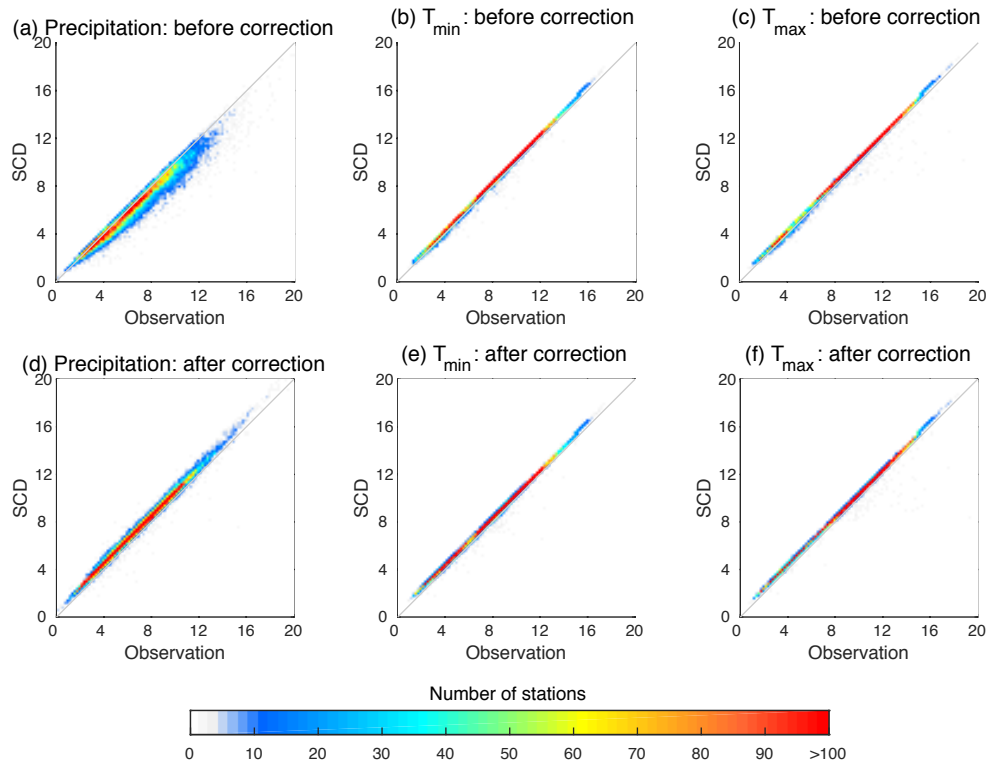
717 Figure 9. Scatter density plots of CC between precipitation from the target station and neighboring stations. For each
 718 target station, the neighboring station with the highest correlation with the target station is selected. X-axis represents
 719 the CC between observed precipitation from target and neighboring stations. Y-axis represents the CC between
 720 estimated precipitation from the target station and the observed precipitation from the neighboring station. Each sub-
 721 figure corresponds to one strategy in Sect. 3.3.2. SCD-1 represents SCD estimates after correction, while SCD-2
 722 replaces estimates by observations. CC is calculated during the overlapped observation period between target and
 723 neighboring stations, and the only exception is SCD-2 which calculates CC using precipitation from target and
 724 neighboring stations during the entire period.



725

726 Figure 10. Similar with Fig. 9, but for T_{\min} .

727 The variability of observations and of the corrected and uncorrected SCDNA estimates (Step-7 in Sect. 3.3.3) are
 728 compared using the standard deviation of the observation period (Fig. 11). The standard deviation of uncorrected
 729 SCDNA precipitation is lower than that of observations, while after correction, the standard deviation agrees very well
 730 with observations. The mean values of standard deviation are 7.36, 6.30, and 7.36 for observations, uncorrected
 731 SCDNA, and corrected SCDNA, respectively. For T_{\min} and T_{\max} , corrected and uncorrected SCDNA estimates both
 732 show consistent variability with observations.



733

734 Figure 11. The standard deviation of observations and SCDNA estimates before and after correction. Data in the
 735 observation period are used.

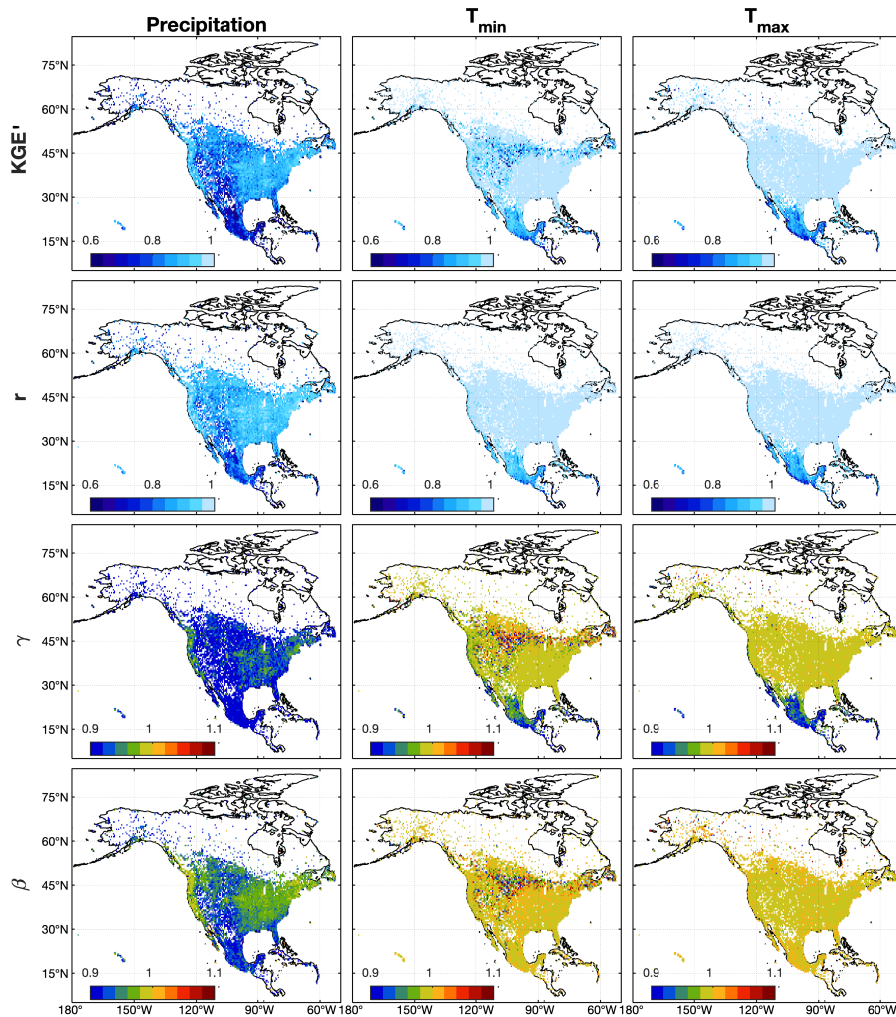
736 4.3 The performance of the serially complete dataset

737 Uncorrected SCDNA estimates show high accuracy in North America (Fig. 12). For precipitation, the median KGE'_i
 738 of all stations is 0.87, and the median values of r , β , and γ are 0.91, 0.92, and 0.96, respectively. The KGE'_i for Mexico
 739 stations generally ranges between 0.6 and 0.8, which is smaller than that in U.S. and southern Canada. Some stations
 740 in Rocky Mountains, Caribbean, Alaska and northern Canada (regions with complex topography or climate), also
 741 show lower KGE'_i for precipitation estimates. The spatial distribution of r is similar with that of KGE'_i , while the
 742 magnitude is higher. According to γ , most stations underestimate precipitation variability which is consistent with Fig.
 743 11; β is generally lower than one in most regions of North America, particularly in Rocky Mountains and Mexico
 744 where SCDNA underestimates precipitation.

745 Estimated temperature shows much higher KGE'_i compared with precipitation. The median KGE'_i and r of T_{min} are
 746 0.97 and 0.99, respectively. For T_{max} , the median of KGE'_i and r are 0.99 and 0.99, respectively. The median γ and β
 747 are both between 0.99 and 1 for T_{min} and T_{max} with small variations, particularly for T_{max} (Fig. 12); the KGE'_i of T_{min}
 748 and T_{max} is lower in Caribbean and Mexico. For T_{min} , the KGE'_i for some stations around 45°N and Rocky Mountains
 749 is lower than surrounding regions although γ is spatially homogeneous for the same region. This is because the mean
 750 T_{min} is close to zero for some stations in this region, resulting in the large magnitude of β and γ . In contrast, T_{max}

751 exhibits homogeneous performance in the same region for all metrics. ~~The discrepancies between T_{\min} and T_{\max} need~~
 752 ~~further investigation.~~

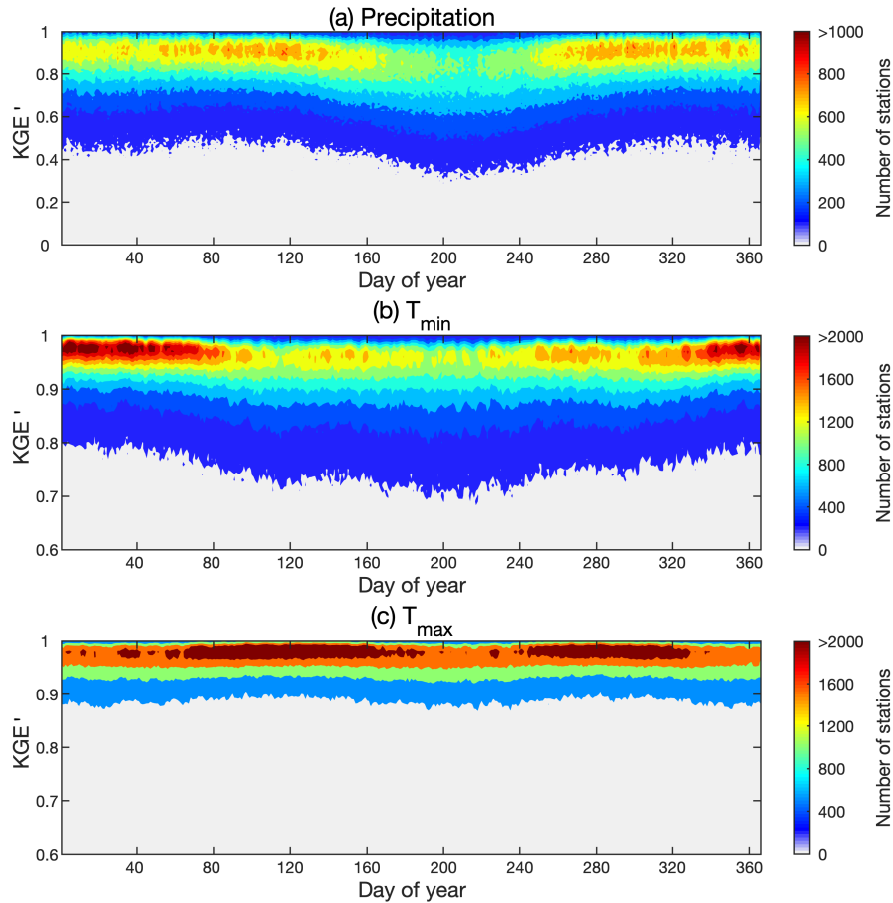
753 Corrected SCDNA estimates (see Step-7; Fig. S9) have higher accuracy than uncorrected estimates (Fig. 12). For
 754 example, the median KGE' for precipitation is improved from 0.87 to 0.90 after correction. The KGE' for T_{\min} and
 755 T_{\max} is also improved but not as significant as precipitation. β equals to one for all stations due to the mean-value
 756 correction. γ for precipitation changes from negative to positive for all stations, whereas magnitude of bias (deviation
 757 from one) is smaller after correction. ~~As a result, t~~he spatial distribution of metrics for T_{\min} is also more homogeneous.
 758 ~~Therefore, the correction procedures are effective.~~



759

760 Figure 12. The spatial distributions of KGE' and its three components (r is CC, β is the bias ratio, and γ is the
 761 variability ratio) for uncorrected SCDNA estimates over North America during the observation period. The maps are
 762 at the resolution of 0.5° . The value for each grid cell is the median value of all stations within this grid cell.

763 The distributions of KGE'_i vary during the year (Fig. 13). For precipitation, more stations show lower KGE'_i during
 764 summer (DOY 150 to 250) than at other times of the year, which may be due to the variability of summertime
 765 convective precipitation. For T_{min} , some stations show lower KGE'_i from DOY 100 to 250. The seasonal variation of
 766 KGE'_i for T_{max} is relatively weak, although KGE'_i is slightly more concentrated at higher level during spring and autumn
 767 than winter and summer. The overall performance of T_{max} is better than T_{min} and precipitation.



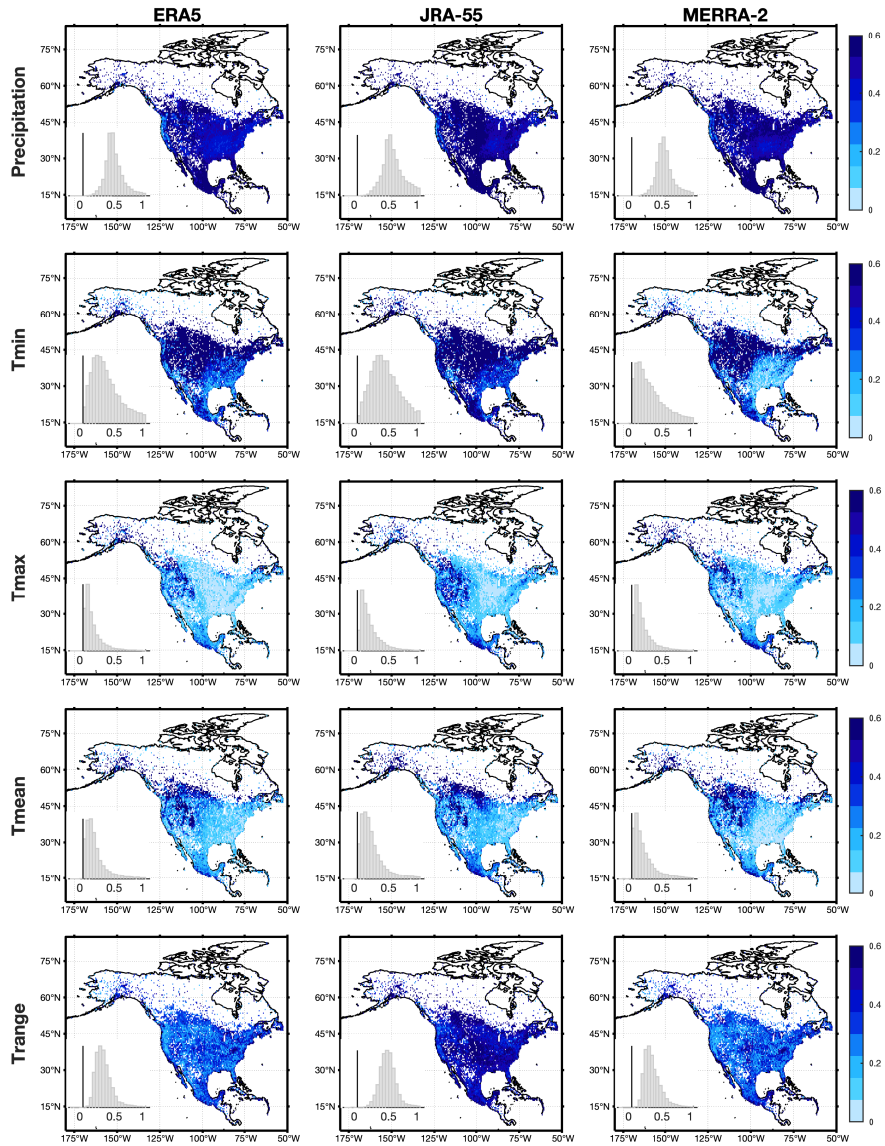
768

769 Figure 13. The distribution of KGE'_i for each day of year for (a) precipitation, (b) T_{min} , and (c) T_{max} . Corrected SCDNA
 770 estimates are used.

771 **4.4 Comparison between the serially complete dataset and gridded products**

772 SCDNA precipitation and temperature are compared with benchmark gridded products to demonstrate whether the
 773 SCDNA is a good choice when station data are unavailable. Actual station observations are used as reference.
 774 Although assessing gridded products using point-scale station data contains uncertainties (Tang et al., 2018a), the
 775 objective of this section is to illustrate their agreement with station observations in lieu of provide an exhaustive
 776 quantitative assessment of their real-world accuracy.

777 Overall, the SCDNA achieves much higher KGE'_i than reanalysis products for all variables (Fig. 14). For precipitation,
 778 the median KGE'_i differences between the SCDNA and ERA5, JRA-55 and MERRA-2 are 0.48, 0.57, and 0.54,
 779 respectively. The corresponding KGE'_i differences for T_{min} are 0.46, 0.61, and 0.36, respectively. The improvement
 780 for T_{max} is smaller, particularly in eastern U.S. where topography is relatively flatter compared with western U.S. The
 781 KGE'_i differences of T_{mean} are lower than T_{min} but higher than T_{max} due to the offset effect. T_{range} suffers little from the
 782 elevation differences between stations and reanalysis grids, and is suitable to demonstrate the differences between
 783 SCDNA and reanalysis products. The median KGE'_i differences for T_{range} between the SCDNA and ERA5, JRA-55
 784 and MERRA-2 are 0.31, 0.48, and 0.31, respectively.

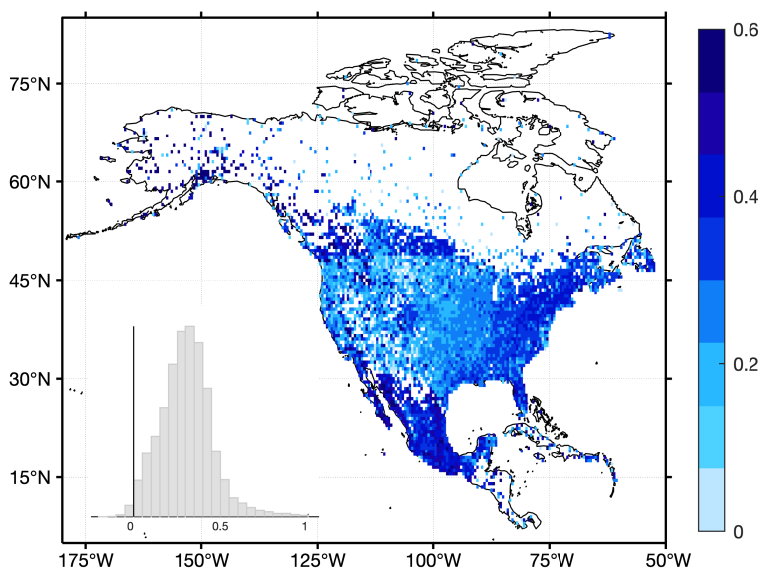


785

786 Figure 14. Spatial distributions of KGE_d differences between SCDNA estimates and three reanalysis products (ERA5,
787 JRA-55, and MERRA-2). The nested histograms show KGE_d differences between the SCDNA and reanalysis products.
788 Corrected SCDNA estimates are used.

789 SCDNA and MSWEP precipitation is compared (Fig. 15). Since MSWEP merges data from numerous stations, the
790 evaluation of MSWEP based on station data is not independent, which could result in the overestimation of its KGE_d.
791 Even so, SCDNA precipitation shows higher KGE_d than MSWEP for 98.97% stations with a median KGE_d difference
792 of 0.31. Fig. 15 shows notable differences between MSWEP and SCDNA at the Canada-USA border and the USA-
793 Mexico border. This is because MSWEP infers gauge reporting time by searching for the highest correlation between
794 gauge data and the temporally shifted reanalysis/satellite estimates (Beck et al., 2019).~~Fig. 15 shows notable~~
795 ~~differences between Canada, U.S. and Mexico~~ The estimated temporal shift could vary with countries, which results
796 in distinct differences of station-based evaluation results along national boundaries ~~which could be due to the~~
797 ~~differences in observation time of stations in different countries~~. The accumulation periods of station and MSWEP
798 precipitation are inconsistent in some cases, which could affect the evaluation of MSWEP (see Sect. 5.1).

799 Note that the evaluation does not indicate that the SCDNA has higher accuracy than the gridded products; rather, the
800 results show that SCDNA is a better substitute than gridded products when station observations are unavailable.



801
802 Figure 15. Spatial distributions of KGE_d differences between SCDNA and MSWEP precipitation. Corrected SCDNA
803 estimates are used.

804 5. Discussion

805 5.1 Observation time of stations

806 Meteorological stations in different countries usually have different local observation time, and stations in the same
807 country may also experience change of observation time (Vincent et al., 2012). Most station databases including those
808 used in this study do not account for reporting-time inconsistencies due to lack of hourly observations and well-
809 documented station metadata. Vincent et al. (2009) examined several methods to adjust the time of daily precipitation
810 observations, which, however, often altered observed precipitation intensity. Beck et al. (2019) inferred the reporting
811 time of daily precipitation observations by calculating SCC between the series of stations and gridded products, which
812 is useful to correct the bias of gridded products. A simple experiment is carried out using the method of Beck et al.
813 (2019) to infer the lag day of station series. For precipitation, 6418 stations show nonnegligible time shift from the
814 reporting date (Fig. S10). However, this method may be unsuitable for temperature because the estimated lag day is
815 mostly zero, and the inferred reporting time cannot be directly applied to adjust station observations.

816 The inconsistent reporting time has different impact on precipitation, T_{\min} , and T_{\max} . For example, if a station records
817 data from 8:00 a.m. on January 1st to 8:00 a.m. on January 2nd, the station will probably use January 2nd as the
818 reporting time. However, two thirds of the 24-h time are within January 1st, indicating that the accumulated
819 precipitation could mostly occur on January 1st. T_{\max} could also occur during the daytime on January 1st, but it is hard
820 to determine on which day T_{\min} occurs, which makes it challenging to adjust precipitation, T_{\min} and T_{\max} at the same
821 time. The difference between universal and local time makes this problem more complicated. Thus, the reporting time
822 of stations is not corrected here due to aforementioned difficulties.

823 5.2 Homogenization

824 Inhomogeneities in station observations are defined as variations that are not caused by weather and climate factors.
825 Long-term station records are often subjected to inhomogeneities due to factors like station re-location, observation
826 time change, instrument change, and surrounding environment change (Venema et al., 2012). Many methods have
827 been developed to identify breakpoints and homogenize station series in annual, monthly or even daily scales (e.g.,
828 Ma et al., 2008; Vincent et al., 2002, 2012). Different methods could generate different estimates of inhomogeneities
829 as shown by many comparison studies (e.g., Beaulieu et al., 2008; Reeves et al., 2007; Venema et al., 2012). The four
830 station databases (Sect. 2.1) used in this study provide original station records without homogenization. The SCDNA
831 would inherit the potential inhomogeneities contained in these databases, and the infilling/reconstruction may also
832 lead to discontinuities. The homogenization of the SCDNA is challenging considering that (1) the dataset covers a
833 broad range of climate, topography, and countries, (2) the number of stations is large and differences between station
834 periods (ranging from 8 to 40 years) are substantial, and (3) whether existing methods are suitable for homogenization
835 of infilling/reconstruction estimates needs exploration. Therefore, homogenization is not carried out in this study,
836 which, however, is an important direction of future studies.

837 **5.3 Limitations of the KGE' statistic**

838 We use KGE' because it incorporates information about correlation, bias, and variability, and hence provides more
839 information on methodological performance than an individual metric. For example, the PCC between temperature
840 estimates and observations is usually close to one and cannot reflect the bias term, while the mean square error is
841 prone to the effect of extreme values (or outliers). However, KGE' also has limitations. For example, the values of
842 KGE' depend on the units of measurement (e.g., Santos et al., 2018) – in our case, the β values for temperature are
843 clearly always close to one if the units of measurement for temperature are in Kelvin. Since these statistics incorrectly
844 indicate very small temperature biases, we used °C for all KGE' calculations in this study, ensuring that β has more
845 leverage in the KGE' statistic. Moreover, and critical for our analysis, the normalization used in the KGE' formula (β
846 and γ) means that the KGE' values are low when the denominators of β and γ are close to zero (e.g., Santos et al.,
847 2018). This problem is especially acute for temperature – for instance, we found that KGE' values were very small for
848 cases where μ_o is close to zero. Nevertheless, the number of cases where μ_o is close to zero is rather small, where
849 ~0.5% of all cases (based on all stations and all DOY) show absolute values of mean T_{min} smaller than 0.1°C. For cases
850 with μ_o close to zero, the ranking based on KGE' is similar to the ranking based on mean absolute error, which
851 means that KGE' can still function as a ranking indicator when its value is low. Further work is needed to both
852 comprehensively evaluate the alternative infilling strategies presented in this paper and evaluate more advanced multi-
853 method merging strategies.

854 **5.4.3 Potential improvement directions**

855 Several steps could be taken to improve the SCDNA. First, the optimal strategy could be different for each station as
856 shown by the results in this study. Therefore, the quality of SCDNA may be further improved by using more
857 infilling/reconstruction methods, which would yield diminishing returns at some point. For example, the long short-
858 term memory (LSTM) could be suitable to impute missing station observations. Optimizing the configuration of
859 various strategies will be necessary to balance computation efficiency and estimation accuracy, particularly when the
860 number of stations is large. Second, some stations suffer from undercatch, which depends on gauge type, precipitation
861 phase, environmental conditions, etc. The bias caused by undercatch can be substantial for stations located in high
862 latitudes and in the mountains (Yang et al., 2005; Scaff et al., 2015). Third, the SCDNA does not distinguish between
863 rainfall and snowfall. Considering that a large part of North America has frequent snowfall in winter, precipitation
864 phase classification will be useful for hydrometeorological studies. Auxiliary data from reanalysis and satellite
865 products could be used to partition precipitation into rain and snow. Finally, although the SCDNA agrees well with
866 station observations, long-term trends are difficult to reconstruct when actual observations are unavailable, meaning
867 the SCDNA may not be suitable for climate trend analysis in the reconstruction period. Some gridded datasets use
868 only stations with long-term records (e.g., (Wood, 2008; Werner et al., 2019) to achieve temporally consistent
869 estimates, whereas such stations are very few. Reasonable trend estimation is challenging but meaningful for SCD.

870 Furthermore, other variables such as wind and humidity observed by stations also suffer from the same problems faced
871 by precipitation and temperature. Future studies should explore whether the current methodology is applicable to other
872 variables. A SCD covering more variables would be useful for research in various fields.

873 **6 Data availability**

874 The SCDNA dataset is available at <https://doi.org/10.5281/zenodo.3735533>~~https://doi.org/10.5281/zenodo.3735534~~
875 (Tang et al., 2020) in netCDF format. The basic variables are station identification, latitude, longitude, elevation, date,
876 and TLR derived in Sect. 3.2. Stations that undergo location merging (Sect. 3.1.1) are identified and all relevant
877 stations are included in the data file. For precipitation, T_{\min} , and T_{\max} , the variables in the netCDF4 file include original
878 station observations, quality flags provided by original station databases, quality flags provided by this study, estimates
879 from 16 strategies, uncorrected SCDNA estimates, corrected SCDNA estimates, the final SCDNA with estimates
880 replaced by observations, data source flags indicating the source of each record in SCDNA (observations or 16
881 strategies), and accuracy metrics (KGE' and its three components) for all estimates (16 strategies and SCDNA).

882 Scripts used to produce the SCDNA are available at <https://github.com/tgq14/GapFill>. The dataset will be regularly
883 updated to cover latest periods.

884 **7 Conclusions**

885 This study developed a daily SCD of precipitation, T_{\min} , and T_{\max} for ~~27280~~27276 stations from 1979 to 2018 over
886 North America (SCDNA). The original station data are compiled from multiple sources and undergo strict quality
887 control. Many stations have nonnegligible fractions of missing values in observation and reconstruction periods. For
888 each station, the infilling and reconstruction are implemented using 16 strategies (quantile mapping, statistical
889 interpolation, and machine learning) based on information from neighboring stations and concurrent reanalysis
890 estimates (ERA5, JRA-55, and MERRA-2). The final SCDNA combines estimates from the 16 strategies and is
891 corrected using station observations. The spatial correlation is preserved and might be slightly inflated. The SCDNA
892 estimates reproduce the variance of original station observations very well, particularly for temperature. The median
893 KGE' of the final precipitation, T_{\min} , and T_{\max} for all stations is 0.90, 0.98, and 0.99, respectively. The comparison
894 with four benchmark gridded products shows that the SCDNA has much better agreement with station observations.
895 The SCDNA will be useful for a variety of hydrometeorological studies in North America.

896

897 **Author contributions:** GT and MC designed the study. GT performed the analyses and wrote the paper. All authors
898 contributed to data analysis, discussions about the methods and results, and paper improvement.

899 **Competing interests:** The authors declare that they have no conflict of interest.

900 **Acknowledgements:** The study is funded by the Global Water Futures (GWF) program in Canada. The authors
 901 appreciate the extensive efforts from the developers of the ground and reanalysis datasets to make their products
 902 available. The authors also thank Zenodo (<https://zenodo.org/>) for publishing our dataset as open access to users.

903 **Appendix A**

904 Table A1. Acronyms used in this paper

Acronym	Full name
ANN	Artificial neural network
APHRODITE	Asian Precipitation-Highly-Resolved Observational Data Integration Towards Evaluation
CC	Correlation coefficient
CDF	Cumulative distribution function
CONUS	Contiguous United States
DEM	Digital elevation model
DOY	Day of year
ECCC	Environment and Climate Change Canada
ERA5	the fifth generation of ECMWF atmospheric reanalyses of the global climate
fD	Fraction of days without precipitation
GHCN-D	Global Historical Climate Network Daily
GSOD	Global Surface Summary of the Day
IDW	Inverse distance weighting
INT	Interpolation
JRA-55	Japanese 55-year Reanalysis
KGE	Kling-Gupta Efficiency
LSTM	Long short-term memory
MAL	Machine learning
MLAD	Multiple regression based on the least absolute deviation criteria
MERIT DEM	Multi-Error-Removed Improved-Terrain digital elevation model
MERRA-2	Modern-Era Retrospective analysis for Research and Applications, Version 2
MRG	Multi-strategy merging
MSWEP	Multi-Source Weighted-Ensemble Precipitation
NR	Revised normal ratio
PCC	Pearson CC
QM	Quantile mapping
QMN	QM using neighboring stations
QMR	Quantile mapping with concurrent reanalysis estimates
RF	Random forest
SCC	Spearman CC

SCDs	Serially complete datasets
TLR	Temperature lapse rate
T_{\max}	Maximum temperature
T_{mean}	Mean temperature
T_{\min}	Minimum temperature
T_{range}	Daily temperature range
U.S.	United States
UTC	Universal Time Coordinated

905

906 **Appendix B**

907 Five types of checks (Durre et al., 2010) are adopted for the quality control of temperature.

908 1. Integrity checks. The first type of integrity check is *a duplication check* to identify duplicated records for time
 909 series in different time periods. The second type of integrity check includes *the streak check* to identify
 910 consecutive identical values and *the frequent-value check* to identify close but not necessarily consecutive
 911 identical values. The *world record exceedance check* sets lower (-89.4°C) and upper (57.7°C) bounds of
 912 temperature.

913 2. Outlier checks, including *the gap check* that examines the frequency distributions for all calendar months, and
 914 the *climatological outlier check* that is based on the traditional z-score (e.g., Hubbard and You, 2005).

915 3. Internal and temporal consistency checks, including *the iterative temperature consistency check*, to ensure some
 916 inherent relationships are abided (e.g., T_{\min} cannot be larger than T_{\max}); *the spike/dip check*, identifies
 917 temperatures which deviate from previous and following days by at least 25°C ; and *the lagged temperature range*
 918 *check*, which identifies abnormally large differences between T_{\min} and T_{\max} during a 3-day time window.

919 4. Spatial consistency checks, including *the regression check* and *the spatial corroboration check*. *The regression*
 920 *check* builds regression relationships between temperature at the target location and selected nearby stations to
 921 determine whether temperature at the target station should be flagged according to regression residuals and
 922 standardized residuals. *The spatial corroboration check* flags temperature at the target station if the value
 923 deviates far from the temperature at neighboring stations.

924 5. Extreme megaconsistency checks to ensure that certain relationships hold for the entire records of stations. For
 925 example, T_{\max} cannot be higher than the lowest T_{\min} for the calendar month, and vice versa.

926 For precipitation, quality control strategies are from three studies. The first part is similar with temperature, but does
 927 not include the third type of checks (internal and temporal consistency checks). The second part is from Hamada et al.
 928 (2011).

- 929 1. Repetition checks. The non-zero check identifies constant daily values ($> 10 \text{ mm d}^{-1}$) that occur for more than
 930 four days. The zero check compares the annual zero-precipitation frequency with its climatological value to spot
 931 unusual frequencies of zero.
- 932 2. Duplicated monthly or sub-monthly record check. The temporal CC and the number of days with equal
 933 precipitation are used to identify whether two different months have the same records caused by human errors.
- 934 3. Z-score-based outlier check. Daily precipitation is flagged if its difference with the mean value from precipitation
 935 within a 15-day window of all years is larger than nine standard deviations. This step is repeated until no outlier
 936 is identified.
- 937 4. Spatiotemporally isolated value check. Extremely large precipitation is identified in both space and time based
 938 on the percentiles of precipitation differences between the target station and neighboring stations within a radius
 939 of 400 km.

940 The third part is from Beck et al. (2019).

- 941 1. Empirical criterion based on the fraction of days without precipitation (fD). This was designed to identify the long
 942 series of erroneous zero precipitation contained in GSOD station records. However, we found that this criterion
 943 misidentifies some acceptable records in GHCN-D. Therefore, the fD -based check is only implemented for GSOD.
- 944 2. Discarding stations with fewer than 15 unique values or more than 99.5% dry records ($<0.5 \text{ mm d}^{-1}$).

945 **References**

- 946 Alexander, L. V., Zhang, X., Peterson, T. C., Caesar, J., Gleason, B., Tank, A. M. G. K., Haylock, M., Collins, D.,
 947 Trewin, B., Rahimzadeh, F., Tagipour, A., Kumar, K. R., Revadekar, J., Griffiths, G., Vincent, L., Stephenson, D. B.,
 948 Burn, J., Aguilar, E., Brunet, M., Taylor, M., New, M., Zhai, P., Rusticucci, M. and Vazquez-Aguirre, J. L.: Global
 949 observed changes in daily climate extremes of temperature and precipitation, *J. Geophys. Res. Atmospheres*, 111(D5),
 950 doi:10.1029/2005JD006290, 2006.
- 951 Anderson, B. T., Wang, J., Salvucci, G., Gopal, S. and Islam, S.: Observed Trends in Summertime Precipitation over
 952 the Southwestern United States, *J. Clim.*, 23(7), 1937–1944, doi:10.1175/2009JCLI3317.1, 2009.
- 953 Beaulieu, C., Seidou, O., Ouarda, T. B. M. J., Zhang, X., Boulet, G. and Yagouti, A.: Intercomparison of
 954 homogenization techniques for precipitation data, *Water Resour. Res.*, 44(2), doi:10.1029/2006WR005615, 2008.
- 955 Beck, H. E., van Dijk, A. I. J. M., Levizzani, V., Schellekens, J., Miralles, D. G., Martens, B. and de Roo, A.: MSWEP:
 956 3-hourly 0.25° global gridded precipitation (1979–2015) by merging gauge, satellite, and reanalysis data, *Hydrol.*
 957 *Earth Syst. Sci.*, 21(1), 589–615, doi:10.5194/hess-21-589-2017, 2017.
- 958 Beck, H. E., Wood, E. F., Pan, M., Fisher, C. K., Miralles, D. G., van Dijk, A. I. J. M., McVicar, T. R. and Adler, R.
 959 F.: MSWEP V2 Global 3-Hourly 0.1° Precipitation: Methodology and Quantitative Assessment, *Bull. Am. Meteorol.*
 960 *Soc.*, 100(3), 473–500, doi:10.1175/BAMS-D-17-0138.1, 2019.
- 961 Breiman, L.: Random Forests, *Mach. Learn.*, 45(1), 5–32, doi:10.1023/A:1010933404324, 2001.

- 962 Cannon, A. J., Sobie, S. R. and Murdock, T. Q.: Bias Correction of GCM Precipitation by Quantile Mapping: How
963 Well Do Methods Preserve Changes in Quantiles and Extremes?, *J. Clim.*, 28(17), 6938–6959, doi:10.1175/JCLI-D-
964 14-00754.1, 2015.
- 965 Che Ghani, N. Z., Abu Hasan, Z. and Tze Liang, L.: Estimation of Missing Rainfall Data Using GEP: Case Study of
966 Raja River, Alor Setar, Kedah, *Adv. Artif. Intell.*, doi:10.1155/2014/716398, 2014.
- 967 Copernicus Climate Change Service (C3S): ERA5: Fifth generation of ECMWF atmospheric reanalyses of the global
968 climate, Copernic. Clim. Change Serv. Clim. Data Store CDS July 2019 <https://cds.climate.copernicus.eu/cdsapphome>,
969 2017.
- 970 Coulibaly, P. and Evora, N. D.: Comparison of neural network methods for infilling missing daily weather records, *J.*
971 *Hydrol.*, 341(1), 27–41, doi:10.1016/j.jhydrol.2007.04.020, 2007.
- 972 Dastorani, M. T., Moghadamnia, A., Piri, J. and Rico-Ramirez, M.: Application of ANN and ANFIS models for
973 reconstructing missing flow data, *Environ. Monit. Assess.*, 166(1), 421–434, doi:10.1007/s10661-009-1012-8, 2010.
- 974 Devi, U., Shekhar, M. S., Singh, G. P., Rao, N. N. and Bhatt, U. S.: Methodological application of quantile mapping
975 to generate precipitation data over Northwest Himalaya, *Int. J. Climatol.*, 39(7), 3160–3170, doi:10.1002/joc.6008,
976 2019.
- 977 Devine, K. A. and Mekis, E.: Field accuracy of Canadian rain measurements, *Atmosphere-Ocean*, 46(2), 213–227,
978 2008.
- 979 Di Luzio, M., Johnson, G. L., Daly, C., Eischeid, J. K. and Arnold, J. G.: Constructing Retrospective Gridded Daily
980 Precipitation and Temperature Datasets for the Conterminous United States, *J. Appl. Meteorol. Climatol.*, 47(2), 475–
981 497, doi:10.1175/2007JAMC1356.1, 2008.
- 982 Di Piazza, A., Conti, F. L., Noto, L. V., Viola, F. and La Loggia, G.: Comparative analysis of different techniques for
983 spatial interpolation of rainfall data to create a serially complete monthly time series of precipitation for Sicily, Italy,
984 *Int. J. Appl. Earth Obs. Geoinformation*, 13(3), 396–408, doi:10.1016/j.jag.2011.01.005, 2011.
- 985 Durre, I., Menne, M. J., Gleason, B. E., Houston, T. G. and Vose, R. S.: Comprehensive Automated Quality Assurance
986 of Daily Surface Observations, *J. Appl. Meteorol. Climatol.*, 49(8), 1615–1633, doi:10.1175/2010JAMC2375.1, 2010.
- 987 Eischeid, J. K., Bruce Baker, C., Karl, T. R. and Diaz, H. F.: The Quality Control of Long-Term Climatological Data
988 Using Objective Data Analysis, *J. Appl. Meteorol.*, 34(12), 2787–2795, doi:10.1175/1520-
989 0450(1995)034<2787:TQCOLT>2.0.CO;2, 1995.
- 990 Eischeid, J. K., Pasteris, P. A., Diaz, H. F., Plantico, M. S. and Lott, N. J.: Creating a Serially Complete, National
991 Daily Time Series of Temperature and Precipitation for the Western United States, *J. Appl. Meteorol.*, 39(9), 1580–
992 1591, doi:10.1175/1520-0450(2000)039<1580:CASCND>2.0.CO;2, 2000.
- 993 Gao, L., Bernhardt, M. and Schulz, K.: Elevation correction of ERA-Interim temperature data in complex terrain,
994 *Hydrol. Earth Syst. Sci.*, 16(12), 4661–4673, doi:10.5194/hess-16-4661-2012, 2012.
- 995 Gao, L., Wei, J., Wang, L., Bernhardt, M., Schulz, K. and Chen, X.: A high-resolution air temperature data set for the
996 Chinese Tian Shan in 1979–2016, *Earth Syst. Sci. Data*, 10(4), 2097–2114, doi:10.5194/essd-10-2097-2018, 2018.
- 997 Gardner, A. S., Sharp, M. J., Koerner, R. M., Labine, C., Boon, S., Marshall, S. J., Burgess, D. O. and Lewis, D.:
998 Near-Surface Temperature Lapse Rates over Arctic Glaciers and Their Implications for Temperature Downscaling, *J.*
999 *Clim.*, 22(16), 4281–4298, doi:10.1175/2009jcli2845.1, 2009.
- 1000 Gelaro, R., McCarty, W., Suárez, M. J., Todling, R., Molod, A., Takacs, L., Randles, C. A., Darmenov, A., Bosilovich,
1001 M. G., Reichle, R., Wargan, K., Coy, L., Cullather, R., Draper, C., Akella, S., Buchard, V., Conaty, A., da Silva, A.

- 1002 M., Gu, W., Kim, G.-K., Koster, R., Lucchesi, R., Merkova, D., Nielsen, J. E., Partyka, G., Pawson, S., Putman, W.,
 1003 Rienecker, M., Schubert, S. D., Sienkiewicz, M. and Zhao, B.: The Modern-Era Retrospective Analysis for Research
 1004 and Applications, Version 2 (MERRA-2), *J. Clim.*, 30(14), 5419–5454, doi:10.1175/jcli-d-16-0758.1, 2017.
- 1005 Gruber, S.: Derivation and analysis of a high-resolution estimate of global permafrost zonation, *The Cryosphere*, 6(1),
 1006 221–233, doi:10.5194/tc-6-221-2012, 2012.
- 1007 Gupta, H. V., Kling, H., Yilmaz, K. K. and Martinez, G. F.: Decomposition of the mean squared error and NSE
 1008 performance criteria: Implications for improving hydrological modelling, *J. Hydrol.*, 377(1–2), 80–91, 2009.
- 1009 Hamada, A., Arakawa, O. and Yatagai, A.: An Automated Quality Control Method for Daily Rain-gauge Data, *Glob.*
 1010 *Environ. Res.*, 15(2), 183–192, 2011.
- 1011 Hasanpour Kashani, M. and Dinpashoh, Y.: Evaluation of efficiency of different estimation methods for missing
 1012 climatological data, *Stoch. Environ. Res. Risk Assess.*, 26(1), 59–71, doi:10.1007/s00477-011-0536-y, 2012.
- 1013 Hubbard, K. G. and You, J.: Sensitivity Analysis of Quality Assurance Using the Spatial Regression Approach—A
 1014 Case Study of the Maximum/Minimum Air Temperature, *J. Atmospheric Ocean. Technol.*, 22(10), 1520–1530,
 1015 doi:10.1175/JTECH1790.1, 2005.
- 1016 Kanda, N., Negi, H. S., Rishi, M. S. and Shekhar, M. S.: Performance of various techniques in estimating missing
 1017 climatological data over snowbound mountainous areas of Karakoram Himalaya, *Meteorol. Appl.*, 25(3), 337–349,
 1018 doi:10.1002/met.1699, 2018.
- 1019 Kemp, W. P., Burnell, D. G., Everson, D. O. and Thomson, A. J.: Estimating Missing Daily Maximum and Minimum
 1020 Temperatures, *J. Clim. Appl. Meteorol.*, 22(9), 1587–1593, doi:10.1175/1520-
 1021 0450(1983)022<1587:EMDMAM>2.0.CO;2, 1983.
- 1022 Kenawy, A. E., López-Moreno, J. I., Stepanek, P. and Vicente-Serrano, S. M.: An assessment of the role of
 1023 homogenization protocol in the performance of daily temperature series and trends: application to northeastern Spain,
 1024 *Int. J. Climatol.*, 33(1), 87–108, doi:10.1002/joc.3410, 2013.
- 1025 Kling, H., Fuchs, M. and Paulin, M.: Runoff conditions in the upper Danube basin under an ensemble of climate
 1026 change scenarios, *J. Hydrol.*, 424, 264–277, 2012.
- 1027 Knowles, N., Dettinger, M. D. and Cayan, D. R.: Trends in Snowfall versus Rainfall in the Western United States, *J.*
 1028 *Clim.*, 19(18), 4545–4559, doi:10.1175/JCLI3850.1, 2006.
- 1029 Kobayashi, S., Ota, Y., Harada, Y., Ebata, A., Moriya, M., Onoda, H., Onogi, K., Kamahori, H., Kobayashi, C., Endo,
 1030 H., Miyaoka, K. and Takahashi, K.: The JRA-55 Reanalysis: General Specifications and Basic Characteristics, *J.*
 1031 *Meteorol. Soc. Jpn. Ser II*, 93(1), 5–48, doi:10.2151/jmsj.2015-001, 2015.
- 1032 Livneh, B., Bohn, T. J., Pierce, D. W., Munoz-Arriola, F., Nijssen, B., Vose, R., Cayan, D. R. and Brekke, L.: A
 1033 spatially comprehensive, hydrometeorological data set for Mexico, the U.S., and Southern Canada 1950–2013, *Sci.*
 1034 *Data*, 2(1), 150042, doi:10.1038/sdata.2015.42, 2015.
- 1035 Longman, R. J., Frazier, A. G., Newman, A. J., Giambelluca, T. W., Schanzenbach, D., Kagawa-Viviani, A., Needham,
 1036 H., Arnold, J. R. and Clark, M. P.: High-Resolution Gridded Daily Rainfall and Temperature for the Hawaiian Islands
 1037 (1990–2014), *J. Hydrometeorol.*, 20(3), 489–508, doi:10.1175/JHM-D-18-0112.1, 2019.
- 1038 Ma, C., Fassnacht, S. R. and Kampf, S. K.: How Temperature Sensor Change Affects Warming Trends and Modeling:
 1039 An Evaluation Across the State of Colorado, *Water Resour. Res.*, 55(11), 9748–9764, 2019.

- 1040 Ma, L., Zhang, T., Li, Q., Frauenfeld, O. W. and Qin, D.: Evaluation of ERA-40, NCEP-1, and NCEP-2 reanalysis air
1041 temperatures with ground-based measurements in China, *J. Geophys. Res.*, 113(D15), doi:10.1029/2007jd009549,
1042 2008.
- 1043 Ma, Y., Hong, Y., Chen, Y., Yang, Y., Tang, G., Yao, Y., Long, D., Li, C., Han, Z. and Liu, R.: Performance of
1044 Optimally Merged Multisatellite Precipitation Products Using the Dynamic Bayesian Model Averaging Scheme Over
1045 the Tibetan Plateau, *J. Geophys. Res. Atmospheres*, 123(2), 814–834, doi:10.1002/2017jd026648, 2018.
- 1046 Maraun, D.: Bias Correction, Quantile Mapping, and Downscaling: Revisiting the Inflation Issue, *J. Clim.*, 26(6),
1047 2137–2143, doi:10.1175/JCLI-D-12-00821.1, 2013.
- 1048 Marshall, S. J., Sharp, M. J., Burgess, D. O. and Anslow, F. S.: Near-surface-temperature lapse rates on the Prince of
1049 Wales Icefield, Ellesmere Island, Canada: implications for regional downscaling of temperature, *Int. J. Climatol.*,
1050 27(3), 385–398, doi:10.1002/joc.1396, 2007.
- 1051 Mekis, É. and Brown, R.: Derivation of an adjustment factor map for the estimation of the water equivalent of snowfall
1052 from ruler measurements in Canada, *Atmosphere-Ocean*, 48(4), 284–293, doi:10.3137/AO1104.2010, 2010.
- 1053 Menne, M. J., Durre, I., Vose, R. S., Gleason, B. E. and Houston, T. G.: An overview of the global historical
1054 climatology network-daily database, *J. Atmospheric Ocean. Technol.*, doi:10.1175/JTECH-D-11-00103.1, 2012.
- 1055 Metcalfe, J. R., Routledge, B. and Devine, K.: Rainfall measurement in Canada: changing observational methods and
1056 archive adjustment procedures, *J. Clim.*, 10(1), 92–101, 1997.
- 1057 Minder, J. R., Mote, P. W. and Lundquist, J. D.: Surface temperature lapse rates over complex terrain: Lessons from
1058 the Cascade Mountains, *J. Geophys. Res.*, 115(D14), doi:10.1029/2009jd013493, 2010.
- 1059 Newman, A. J., Clark, M. P., Craig, J., Nijssen, B., Wood, A., Gutmann, E., Mizukami, N., Brekke, L. and Arnold, J.
1060 R.: Gridded Ensemble Precipitation and Temperature Estimates for the Contiguous United States, *J. Hydrometeorol.*,
1061 16(6), 2481–2500, doi:10.1175/JHM-D-15-0026.1, 2015.
- 1062 Newman, A. J., Clark, M. P., Longman, R. J., Gilleland, E., Giambelluca, T. W. and Arnold, J. R.: Use of Daily Station
1063 Observations to Produce High-Resolution Gridded Probabilistic Precipitation and Temperature Time Series for the
1064 Hawaiian Islands, *J. Hydrometeorol.*, 20(3), 509–529, doi:10.1175/JHM-D-18-0113.1, 2019.
- 1065 Papalexiou, S. M. and Montanari, A.: Global and regional increase of precipitation extremes under global warming,
1066 *Water Resour. Res.*, 55(6), 4901–4914, 2019.
- 1067 Papalexiou, S. M., AghaKouchak, A., Trenberth, K. E. and Foufoula-Georgiou, E.: Global, regional, and megacity
1068 trends in the highest temperature of the year: Diagnostics and evidence for accelerating trends, *Earth's Future*, 6(1),
1069 71–79, 2018.
- 1070 Pappas, C., Papalexiou, S. M. and Koutsoyiannis, D.: A quick gap filling of missing hydrometeorological data, *J.*
1071 *Geophys. Res. Atmospheres*, 119(15), 9290–9300, 2014.
- 1072 Paulhus, J. L. H. and Kohler, M. A.: Interpolation of missing precipitation records, *Mon. Weather Rev.*, 80(8), 129–
1073 133, doi:10.1175/1520-0493(1952)080<0129:IOMPR>2.0.CO;2, 1952.
- 1074 Pielke Sr, R., Nielsen-Gammon, J., Davey, C., Angel, J., Bliss, O., Doesken, N., Cai, M., Fall, S., Niyogi, D. and
1075 Gallo, K.: Documentation of uncertainties and biases associated with surface temperature measurement sites for
1076 climate change assessment, *Bull. Am. Meteorol. Soc.*, 88(6), 913–928, 2007.
- 1077 Ramos-Calzado, P., Gómez-Camacho, J., Pérez-Bernal, F. and Pita-López, M. F.: A novel approach to precipitation
1078 series completion in climatological datasets: application to Andalusia, *Int. J. Climatol.*, 28(11), 1525–1534,
1079 doi:10.1002/joc.1657, 2008.

- 1080 Reeves, J., Chen, J., Wang, X. L., Lund, R. and Lu, Q. Q.: A Review and Comparison of Change-
1081 point Detection Techniques for Climate Data, *J. Appl. Meteorol. Climatol.*, 46(6), 900–915, doi:10.1175/JAM2493.1, 2007.
- 1082 Rubin, D. B.: Inference and missing data, *Biometrika*, 63(3), 581–592, doi:10.1093/biomet/63.3.581, 1976.
- 1083 Santos, L., Thirel, G. and Perrin, C.: Technical note: Pitfalls in using log-transformed flows within the KGE criterion,
1084 *Hydrol. Earth Syst. Sci.*, 22, 4583–4591, doi:10.5194/hess-22-4583-2018, 2018.
- 1085 Sattari, M.-T., Rezazadeh-Joudi, A. and Kusiak, A.: Assessment of different methods for estimation of missing data
1086 in precipitation studies, *Hydrol. Res.*, 48(4), 1032–1044, doi:10.2166/nh.2016.364, 2017.
- 1087 Scaff, L., Yang, D., Li, Y. and Mekis, E.: Inconsistency in precipitation measurements across the Alaska–Yukon
1088 border, *The Cryosphere*, 9(6), 2417–2428, doi:10.5194/tc-9-2417-2015, 2015.
- 1089 Serrano-Notivoli, R., Beguería, S. and Luis, M. de: STEAD: a high-resolution daily gridded temperature dataset for
1090 Spain, *Earth Syst. Sci. Data*, 11(3), 1171–1188, doi:https://doi.org/10.5194/essd-11-1171-2019, 2019.
- 1091 Shepard, D.: A two-dimensional interpolation function for irregularly-spaced data, in *Proceedings of the 1968 23rd*
1092 *ACM national conference*, pp. 517–524, ACM., 1968.
- 1093 Simolo, C., Brunetti, M., Maugeri, M. and Nanni, T.: Improving estimation of missing values in daily precipitation
1094 series by a probability density function-preserving approach, *Int. J. Climatol.*, 30(10), 1564–1576,
1095 doi:10.1002/joc.1992, 2010.
- 1096 Stooksbury, D. E., Idso, C. D. and Hubbard, K. G.: The Effects of Data Gaps on the Calculated Monthly Mean
1097 Maximum and Minimum Temperatures in the Continental United States: A Spatial and Temporal Study, *J. Clim.*,
1098 12(5), 1524–1533, doi:10.1175/1520-0442(1999)012<1524:TEODGO>2.0.CO;2, 1999.
- 1099 Tang, G., Behrangi, A., Long, D., Li, C. and Hong, Y.: Accounting for spatiotemporal errors of gauges: A critical step
1100 to evaluate gridded precipitation products, *J. Hydrol.*, 559, 294–306, doi:10.1016/j.jhydrol.2018.02.057, 2018a.
- 1101 Tang, G., Behrangi, A., Ma, Z., Long, D. and Hong, Y.: Downscaling of ERA-Interim Temperature in the Contiguous
1102 United States and Its Implications for Rain–Snow Partitioning, *J. Hydrometeorol.*, 19(7), 1215–1233,
1103 doi:10.1175/jhm-d-18-0041.1, 2018b.
- 1104 Tang, G., Clark, M. P., Newman, A. J., Wood, A. W., Papalexiou, S. M., Vionnet, V., Whitfield, P. H.: SCDNA: a
1105 serially complete precipitation and temperature dataset for North America from 1979 to 2018 [Dataset], Zenodo,
1106 https://doi.org/10.5281/zenodo.3735533, 2020.
1107
- 1108 Tang, Q., Wood, A. W. and Lettenmaier, D. P.: Real-Time Precipitation Estimation Based on Index Station Percentiles,
1109 *J. Hydrometeorol.*, 10(1), 266–277, doi:10.1175/2008JHM1017.1, 2009.
- 1110 Teegavarapu, R. S. V. and Chandramouli, V.: Improved weighting methods, deterministic and stochastic data-driven
1111 models for estimation of missing precipitation records, *J. Hydrol.*, 312(1), 191–206,
1112 doi:10.1016/j.jhydrol.2005.02.015, 2005.
- 1113 Ustaoglu, B., Cigizoglu, H. K. and Karaca, M.: Forecast of daily mean, maximum and minimum temperature time
1114 series by three artificial neural network methods, *Meteorol. Appl.*, 15(4), 431–445, doi:10.1002/met.83, 2008.
- 1115 Venema, V. K. C., Mestre, O., Aguilar, E., Auer, I., Guijarro, J. A., Domonkos, P., Vertacnik, G., Szentimrey, T.,
1116 Stepanek, P., Zahradnicek, P., Viarre, J., Müller-Westermeier, G., Lakatos, M., Williams, C. N., Menne, M. J., Lindau,
1117 R., Rasol, D., Rustemeier, E., Kolokythas, K., Marinova, T., Andresen, L., Acquaotta, F., Fratianni, S., Cheval, S.,
1118 Klancar, M., Brunetti, M., Gruber, C., Prohom Duran, M., Likso, T., Esteban, P. and Brandsma, T.: Benchmarking
1119 homogenization algorithms for monthly data, *Clim. Past*, 8(1), 89–115, doi:10.5194/cp-8-89-2012, 2012.

- 1120 Vicente-Serrano, S. M., Saz-Sanchez, M. A. and Cuadrat, J. M.: Comparative analysis of interpolation methods in the
 1121 middle Ebro Valley (Spain): application to annual precipitation and temperature, *Clim. Res.*, 24(2), 161–180, doi:DOI
 1122 10.3354/cr024161, 2003.
- 1123 Vincent, L. A., Zhang, X., Bonsal, B. R. and Hogg, W. D.: Homogenization of Daily Temperatures over Canada, *J.*
 1124 *Clim.*, 15(11), 1322–1334, doi:10.1175/1520-0442(2002)015<1322:HODTOC>2.0.CO;2, 2002.
- 1125 Vincent, L. A., Milewska, E. J., Hopkinson, R. and Malone, L.: Bias in Minimum Temperature Introduced by a
 1126 Redefinition of the Climatological Day at the Canadian Synoptic Stations, *J. Appl. Meteorol. Climatol.*, 48(10), 2160–
 1127 2168, doi:10.1175/2009JAMC2191.1, 2009.
- 1128 Vincent, L. A., Wang, X. L., Milewska, E. J., Wan, H., Yang, F. and Swail, V.: A second generation of homogenized
 1129 Canadian monthly surface air temperature for climate trend analysis, *J. Geophys. Res. Atmospheres*, 117(D18),
 1130 doi:10.1029/2012JD017859, 2012.
- 1131 Wambua, R. M., Mutua, B. M. and Raude, J. M.: Prediction of Missing Hydro-Meteorological Data Series Using
 1132 Artificial Neural Networks (ANN) for Upper Tana River Basin, Kenya, *Am. J. Water Resour.*, 4(2), 35–43,
 1133 doi:10.12691/ajwr-4-2-2, 2016.
- 1134 Wang, X. L., Xu, H., Qian, B., Feng, Y. and Mekis, E.: Adjusted daily rainfall and snowfall data for Canada,
 1135 *Atmosphere-Ocean*, 55(3), 155–168, 2017.
- 1136 Werner, A. T., Schnorbus, M. A., Shrestha, R. R., Cannon, A. J., Zwiers, F. W., Dayon, G. and Anslow, F.: A long-
 1137 term, temporally consistent, gridded daily meteorological dataset for northwestern North America, *Sci. Data*, 6(1), 1–
 1138 16, doi:10.1038/sdata.2018.299, 2019.
- 1139 Whitfield, P. H.: Climate Station Analysis and Fitness for Purpose Assessment of 3053600 Kananaskis, Alberta,
 1140 *Atmosphere-Ocean*, 52(5), 363–383, doi:10.1080/07055900.2014.946388, 2014.
- 1141 Woldesenbet, T. A., Elagib, N. A., Ribbe, L. and Heinrich, J.: Gap filling and homogenization of climatological
 1142 datasets in the headwater region of the Upper Blue Nile Basin, Ethiopia, *Int. J. Climatol.*, 37(4), 2122–2140,
 1143 doi:10.1002/joc.4839, 2017.
- 1144 Wood, A. W.: The University of Washington Surface Water Monitor: An experimental platform for national
 1145 hydrologic assessment and prediction, in 22nd Conf. on Hydrology., 2008.
- 1146 Yamazaki, D., Ikeshima, D., Tawatari, R., Yamaguchi, T., O’Loughlin, F., Neal, J. C., Sampson, C. C., Kanae, S. and
 1147 Bates, P. D.: A high-accuracy map of global terrain elevations, *Geophys. Res. Lett.*, 44(11), 5844–5853,
 1148 doi:10.1002/2017GL072874, 2017.
- 1149 Yang, D., Kane, D., Zhang, Z., Legates, D. and Goodison, B.: Bias corrections of long-term (1973-2004) daily
 1150 precipitation data over the northern regions, *Geophys. Res. Lett.*, 32(19), n/a-n/a, doi:10.1029/2005gl024057, 2005.
- 1151 Yatagai, A., Kamiguchi, K., Arakawa, O., Hamada, A., Yasutomi, N. and Kitoh, A.: APHRODITE: Constructing a
 1152 Long-Term Daily Gridded Precipitation Dataset for Asia Based on a Dense Network of Rain Gauges, *Bull. Am.*
 1153 *Meteorol. Soc.*, 93(9), 1401–1415, doi:10.1175/bams-d-11-00122.1, 2012.
- 1154 Young, K. C.: A Three-Way Model for Interpolating for Monthly Precipitation Values, *Mon. Weather Rev.*, 120(11),
 1155 2561–2569, doi:10.1175/1520-0493(1992)120<2561:ATWMFI>2.0.CO;2, 1992.
- 1156